



BELBaR

(Contract Number: FP7 295487)

Progress Report on erosion processes under flowing water conditions

DELIVERABLE D2.2

Author(s):

Ivars Neretneiks, KTH

Luis Moreno, KTH

Ursula Alonso, Ciemat

Tiziana Missana, Ciemat

Tim Schatz, B+Tech

Radek Červinka, UJV

Patrik Sellin, SKB (editor)

Reporting period: 01/03/12 – 29/02/16

Date of issue of this report: 23/09/13

Start date of project: 01/03/12

Project co-funded by the European Commission under the Seventh Euratom Framework Programme for Nuclear Research & Training Activities (2007-2011)

Dissemination Level

PU

Public

Duration: 48 Months

DISTRIBUTION LIST

Name	Number of copies	Comments
Christophe Davies (EC) BELBaR participants		

Table of Contents

1	BELBaR Deliverable 2.2.....	4
2	Erosion processes under flowing water conditions: KTH.....	5
2.1	Introduction.....	5
2.2	Summary of main mechanisms and models	5
2.2.1	Dynamic model for gel expansion and sol formation	6
2.3	Gel viscosity and flow of gel /sol	8
2.4	Potential effects in real bentonites	10
2.5	Erosion experiments.....	13
2.6	Calcium dominated smectites	18
2.7	Discussion	19
2.8	References.....	19
3	Erosion experiments under flow conditions: CIEMAT.....	21
4	Erosion processes under flowing water conditions (B+Tech)	26
4.1	Background.....	26
4.2	Response to flow velocity and flow interruption	26
4.3	Fate of accessory minerals	29
4.4	Effect of fracture geometry	31
4.5	References	31
5	Bentonite erosion into the granite fracture during the saturation phase ÚJV Řež.....	32
5.1	Introduction.....	32
5.2	Rokle bentonite	32
5.3	Experimental set-up	33
5.4	Results	34

1 BELBaR Deliverable 2.2

The current report contains individual contributions from a number of BELBaR partners concerning erosion processes under flowing water conditions. Each contribution is presented in a separate chapter.

The report describes the current progress at about a quarter of the project time. Therefore, no summary or integrated conclusions are presented.

2 Erosion processes under flowing water conditions: KTH

Ivars Neretnieks, Luis Moreno

2.1 Introduction

The objective of WP 2 is to understand the main mechanisms of erosion of clay particles from the bentonite surface and to quantify the maximum extent of the possible erosion under different physico-chemical conditions.

One aim of this contribution to the progress report is to summarize our present understanding of erosion processes under flowing water conditions and to point out where there is still lacking information of potential importance to quantitatively model erosion.

2.2 Summary of main mechanisms and models

Erosion of the fine smectite particles from compacted bentonite can have several causes. The main are

Very high flowrates past the bentonite gel can shear off particles by physical forces.

In low salinity waters repulsive forces between smectite particles can expand the particles in the gel so that they eventually are so far from each other that they form a stable sol with low viscosity. A dilute gel and especially a sol can flow as a liquid if the viscosity of the gel is low and the hydraulic gradient is high.

We are mainly concerned with the latter two mechanisms. The gel expansion and sol formation is discussed first. The forces that act on the particles are repulsion forces caused by the diffuse layer of cations that are present to compensate the inherent negative charge of the smectite particles. For a given distance between particles this force strongly increases, the lower the ionic strength is of the pore water. It is called the diffuse double layer force, DDL. The always present attractive van der Waals force, vdW, is practically independent of water composition. Depending on the water composition there may be distance at which these forces balance each other. A compact gel would expand up the force balance point and not further. A stable gel would result if no other forces influence the particles. The water composition at which such a balance no longer can be reached, i.e. when the repulsive DDL force will be greater than the vdW force is called the critical coagulation concentration, CCC. Below the CCC, smectite in large body of water would expand forever if not restrained by gravity. There are also other forces that influence the gel/sol properties and behavior.

Figure 2-1 shows a fracture intersecting the canister deposition hole, which is filled with compacted bentonite. The bentonite, when wetted, swells out into the fracture. It has a very high swelling pressure when highly compacted, but the swelling pressure decreases with decreasing bentonite density. The smectite particles are pulled and pushed into the water that seeps in the fracture by the different forces acting on the particles. If the pore water is below the CCC the particles at the bentonite/water interface can diffuse into the moving water and be carried away. There is also a region where the gel/sol has so low a particle concentration that it is little more viscous than water and can flow away. The loss of particles is thus influenced both by particle diffusion and by advective flow of the dilute gel/sol. For both mechanisms, the flowrate of water and gel in the fracture will set the total rate of loss.

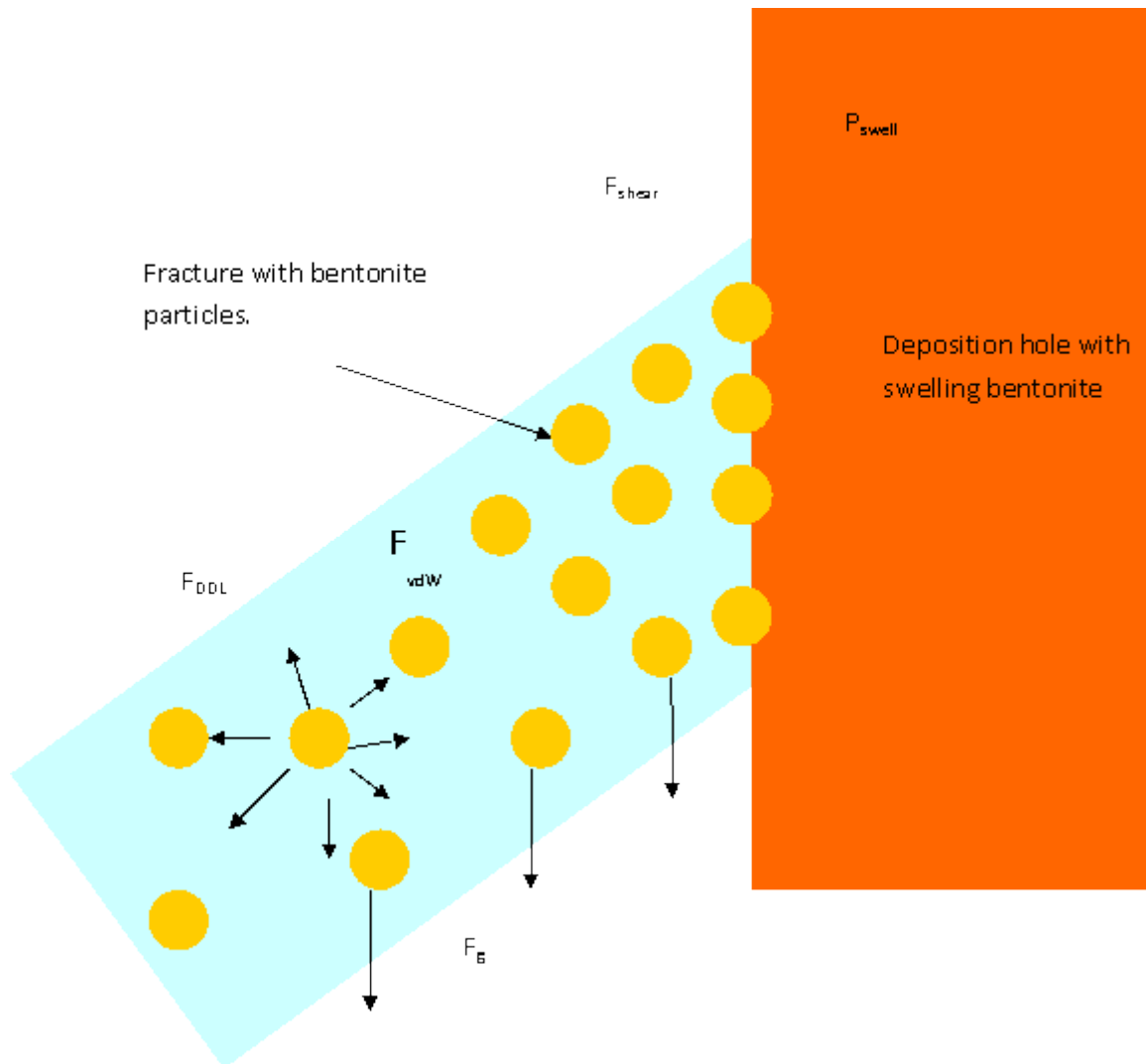


Figure 2-1 Schematic of forces acting on the bentonite in a deposition hole and fracture.

2.2.1 Dynamic model for gel expansion and sol formation

The expansion is a dynamic process. When there remains a net force between the particles they will want to move to decrease the force. In any movement there will be the opposite movement of water to fill the void vacated by the particle. The friction force between a particle and water will restrain the rate of movement of the particles. By balancing these forces, including gravity and particle movement by thermal energy (Brownian movement) a dynamic model was devised for gel/sol expansion by Liu et al (2009a). It was found that the expansion can be described as diffusion of the smectite particles in water. The diffusion coefficient D_F strongly depends on the water composition and the smectite particle concentration. We will describe the particle concentration by the volume fraction of smectite in the gel/sol. The diffusion equation can be used to model the rate of expansion and sol formation. It also has led to a new way of assessing the CCC, which gives order(s) of magnitude better values of CCC than the DLVO theory, (Liu et al 2009b). An example of the diffusivity function is shown in Figure 2-2.

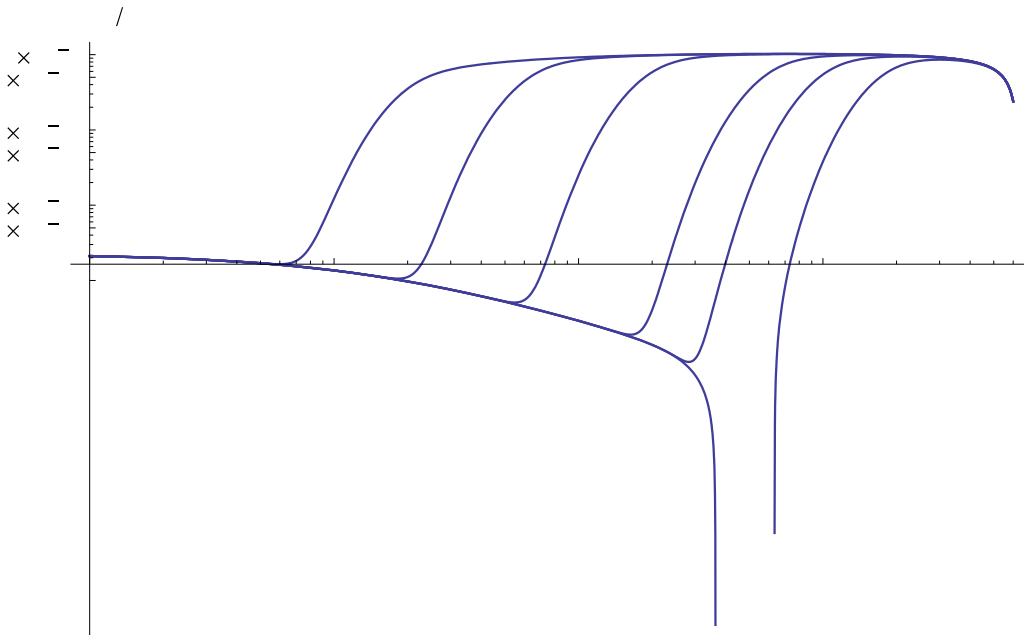


Figure 2-2 Diffusivity function for smectite 300 nm diameter sheets for monovalent ions. The curves from left to right are for 0.01, 0.1, 1, 10, 50 and 100 mM ion for $z=1$, $\delta_p=10^{-9}$ m and $\sigma_0=-0.131$ C/m²

Figure 2-2 shows the diffusivity function for different ion concentrations. To the left the diffusivity is that of individual particles due to Brownian motion and is about 10^{-13} m²/s. For 0.01 mM this applies up to $\phi=0.0006$. At higher particle concentrations the DDL forces start to become noticeable and D_f increases rapidly. It levels off at about 10^{-9} m²/s for all ion concentrations. At an ion concentration just above 50 mM the DDL forces become weaker than the vdW forces and D_f becomes negative at ϕ around 0.05. This means that the particles will move closer to each other instead of diffusing away from each other and will stabilize at a distance where the sum of the interaction energies is minimum. The ion concentration at which this happens is the CCC. This is a way of understanding the CCC phenomenon and predicts the CCC much better than the DLVO theory does for sodium as well as for calcium (Liu et al. 2009b). They found that the CCC depends not only on the surface charge density and the charge of the counterion but also on the thickness of the particles and of the surface area of the particles. For monovalent ions the CCC is predicted to lie between 40 and 100 mM for thin (1.2 nm thick) particles larger than 10000 (nm)². The CCC increases with decreasing particle size. For twice as thick particles the CCC decrease by about half.

With divalent counterions the CCC is predicted to lie between 0.7 and 2 mM for 15 nm thick particles (stacks) larger than 10000 (nm)² and half that for twice as thick particles. This agrees well with observed values. The traditional DLVO theory predicts about two orders of magnitude larger CCC.

The diffusion equation can be used to model the expansion of a smectite gel in water. An example of such modelling is shown in Figure 2-3.

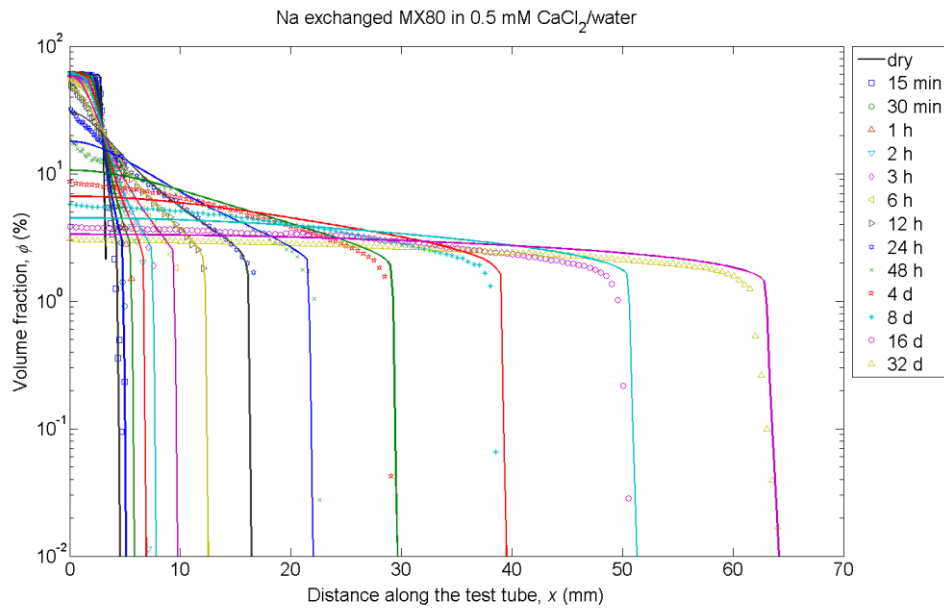


Figure 2-3 Sodium exchanged bentonite in 0.5 mM CaCl₂. Logarithmic scale

Figure 2-3 shows the expansion of a compacted Na-homoionic smectite expanding upwards in a test tube, the marks. The experiments are reported in Dvinskikh and Furó (2009) and Dvinskikh et al. (2009). Model predictions using the dynamic model are given by the full lines. The data used in the modelling are taken from independent information of the smectite properties. No parameter values in the model have been adjusted. The water composition is below the CCC. The particle concentration is shown on a logarithmic scale. It is seen that the particle concentration at the expanding front drops very sharply. The particles attempt to diffuse downstream but are overtaken by the expanding gel compressing the front. However, for the longer times the front moves slower and slower and the diffusion makes itself felt. This is clearly seen in the figure for the longest times. The shape and width of the diffuse front deviates somewhat from that expected for a system with equally sized particles.

The predictions are surprisingly good. It should be noted, however, that the experiment are performed with a highly purified homo-ionic smectite and that there are no other mineral particles present. This is in contrast to the commercial bentonites considered for use in the repositories. These contain not only sodium as charge compensating ions but also Ca, K, Mg and traces of other elements. Furthermore the bentonites contain several tens of percent of accessory minerals such as quartz, feldspar, etc.

2.3 Gel viscosity and flow of gel /sol

The flow velocity of the gel/sol in the fracture depends on the hydraulic gradient and the viscosity of the gel/sol. The viscosity of a dilute sol is expected to be little influenced by the presence of the smectite particles but it will increase with the particle concentration and eventually behave much differently from a Newtonian fluid. When particles come close to each other and “touch” each other the gel becomes increasingly rigid.

The smectite particles are very thin, coin-like, and rotate by the thermal motion. The notion of co-volume has been proposed which describes the size of the particle as the sphere, which the particle needs to rotate in. Somewhat oversimplified, but illustrative, one can think of the gel/sol as follows. When the co-volume spheres start to touch the viscosity becomes increasingly less Newtonian and a minimum shear force is needed to start any movement. For the charged smectite particles with a diffuse double layer of ions this can be assumed to increase the diameter of the particle by some distance proportional to the thickness of the DDL. This is illustrated in Figure 2-4.

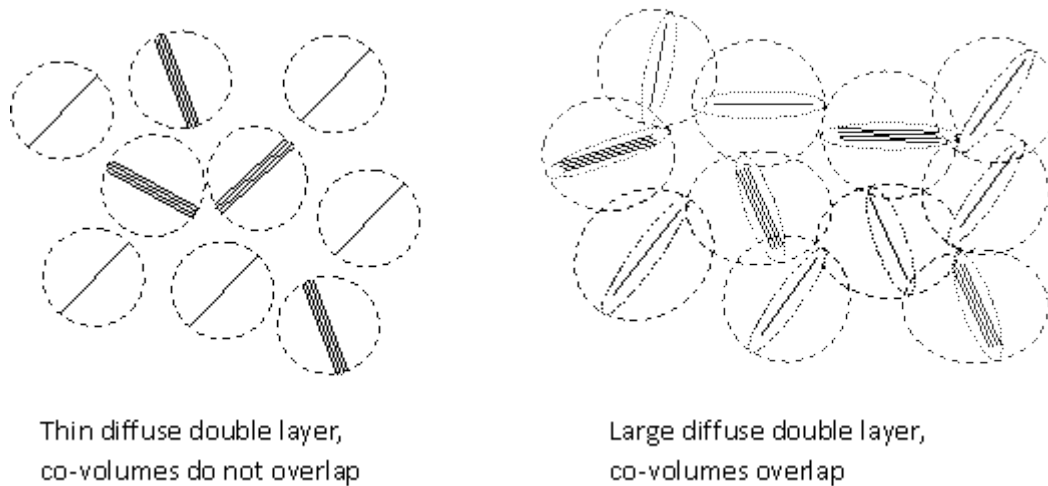


Figure 2-4 Illustration of co-volume with and without impact of diffuse layer for a given volume fraction. The extent of the diffuse layer is shown as dotted oval in the right figure.

It has been found that a very simple relation between the relative viscosity of the gel/sol and the co-volume fraction gives a good correlation for different water compositions. This is illustrated in Figure 2-5, (Liu, 2011). The largest real smectite volume fraction in the figure is 0.9 %. At larger smectite volume fractions the gel becomes increasingly non-Newtonian and increasing stronger shear force is needed to start any movement. Birgersson et al (2009) present a series of rheological experiments with different clays and at different volume fractions.

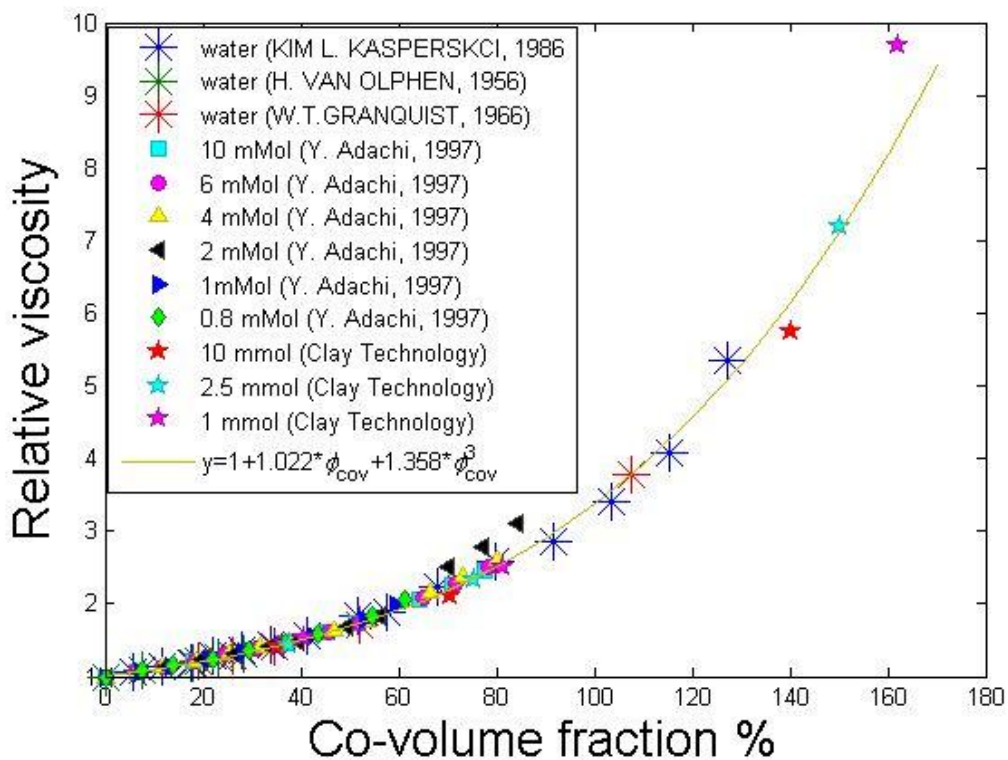


Figure 2-5 Relative viscosity as a function of co-volume fraction from different sources.

With the low shear stresses expected in the fractures with seeping water it is expected that the gel would become practically immobile when the volume fraction is somewhere around 1-2 %.

2.4 Potential effects in real bentonites

There are a number of phenomena expected in a repository situation that are not accounted for in any available models. There is reason to believe that several such phenomena and mechanisms can have a strong impact on the erosion under repository conditions. Some potentially important phenomena are illustrated below. The erosion process of a commercial bentonite can be visualised as shown in Figure 2-6 and Figure 2-7.

The accessory minerals in commercial bentonites, sometimes called detritus material, do not have much electrical charge and the particles are often considerably larger than the smectite particles. This material can be thought of as very fine sand. These particles are much less influenced by the DDL forces than the smectite particles because of their different electrical charge properties and because they in general consists of much larger particles. It is envisaged that as the clay gel expands out into the fracture it will carry with it the small sand particles. Where the gel has expanded so much that it forms a sol, i.e. where the individual smectite particles no longer have strong repulsion forces between them and move essentially randomly and independently of each other propelled by thermal forces (Brownian diffusion), they no more carry the sand particles with them. These are left behind and gradually build up a porous sand bed with essentially stagnant water. The smectite particles now have to move through the sand bed to reach the mobile water. As more smectite is lost, the sand bed keeps increasing in size. The transport of the smectite particles will gradually slow down and may even totally stop when the sand bed is compressed and forms pores less than 300 nm. This is called straining. The particle size distribution of the detritus material should be such that it overlaps with that of the smectite particles for the straining to be effective.

Even if the sand bed does not fully strain the smectite particles, it will slow down smectite particle movement as well as the exchange of solutes between the seeping groundwater and the pore water in the bentonite inside the sand bed. The longer the sand region is the longer distance ions and smectite have to diffuse, which limits the rate of mass transfer. The loss of CCC determining ions will slow down and may eventually become the rate-determining step for the colloid formation. When the loss of charge compensation ions from the more concentrated pore water to the very dilute seeping water in the fracture slows down the concentration at the gel/sol/water interface can creep up above CCC and erosion would stop.

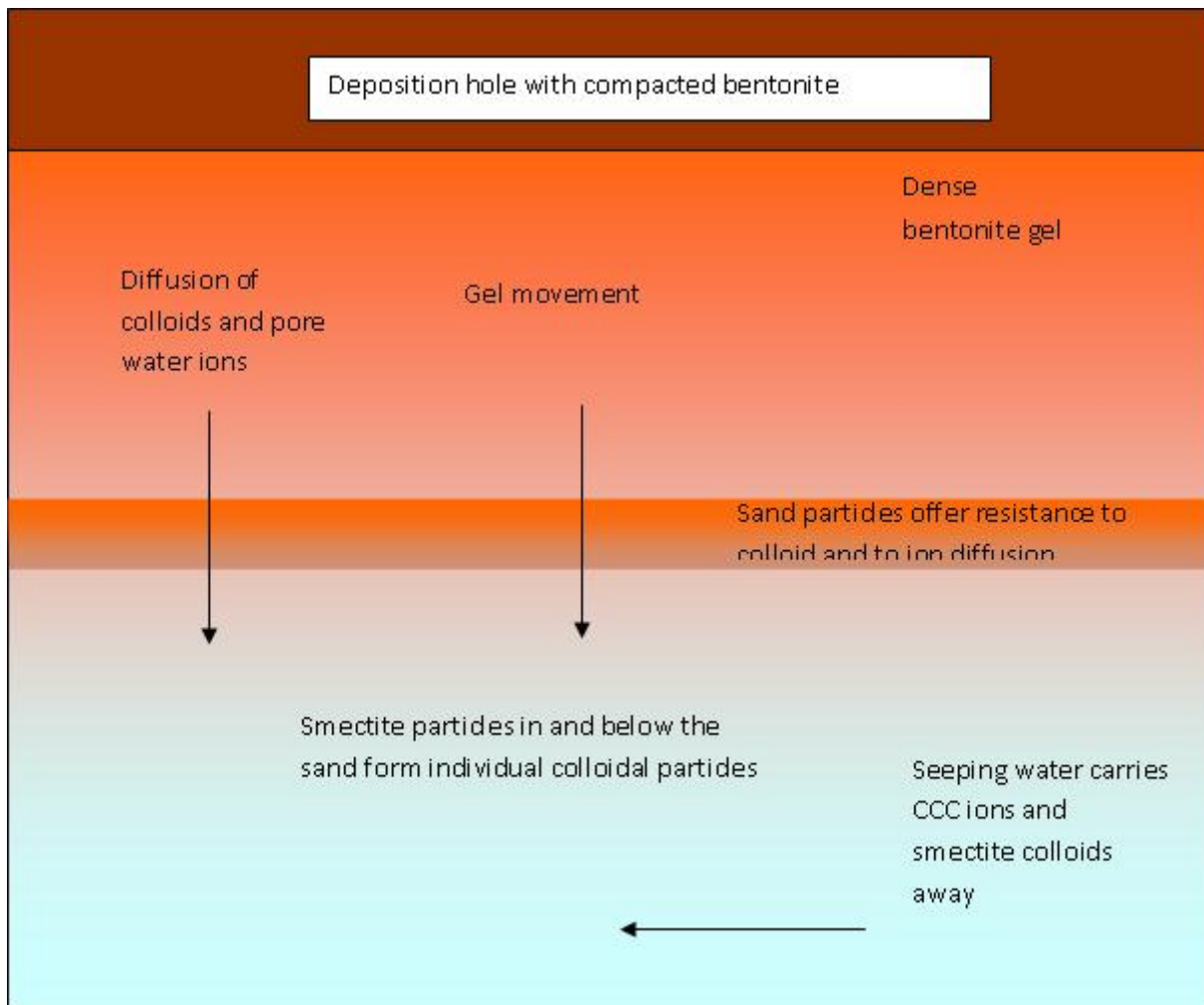


Figure 2-6 Bentonite gel expands downwards from the deposition hole into and in a fracture. Smectite colloids are released from the gel, move through the sand bed and are carried away by the seeping water.

Figure 2-6 illustrates the expansion of the gel in a fracture, the formation of the sand bed and the transport of solutes and colloids through it. At present, we only discuss the case when the pore water is below the CCC in the region around the gel/water interface although it may be above the CCC further into the buffer. DDL forces expand the bentonite into the fracture. The fracture is slanting and gravity will therefore pull back upward expanding particles but pull them downwards into the water at the lower end of the intersection with the deposition hole. The sand particles are left behind when the gel turns to a sol and form a porous bed through which the smectite particles have to pass. This slows down the flux of the smectite particles. In addition, the sand and the gel will slow down the diffusion of ions from the pore water in the gel as the particles form a diffusion barrier with their stagnant water. The sand will be pushed outward in the fracture by the swelling gel but will be restrained by friction and trapping in narrow passages in the fracture. Larger particles will also be physically hindered (strained) from entering and moving far in narrow fractures. This could in turn help to strain smaller particles that get stuck and so on. The particle size distribution in relation to the fracture aperture distribution will determine how far the particles can migrate before clogging the fracture. The particle size distribution of the detritus material overlaps that of fracture apertures and straining and clogging is expected to be potentially important mechanisms that can decrease or even stop erosion.

The thicker the sand bed becomes the more difficult it will be for it to move further out into the fracture. It is also expected that a sand bed will form in the deposition hole at the mouth of the fracture because the expansion into the fracture is increasingly slowed down by friction and

straining. This sand bed will be compressed and compacted by the swelling clay. The sand bed at the mouth of the fracture as well as in the fracture itself will grow with time but the rate of growth will decrease as less and less smectite particles can negotiate paths through the narrow pores of the bed. This has been experimentally shown in laboratory tests with artificially formed mm thick filter beds (Richards and Neretnieks 2010).

In fractures with downward facing component, the sand particles can be pulled downward by gravity contributing to the loss of such particles, as shown in Figure 2-7. Hypothetically the whole downward facing fracture could be filled with such sedimenting sand particles if straining has not set a limit beforehand. The water flowrate will slow down in the fracture now filled with particles and its carrying capacity of smectite particle will decrease.

The solubilised smectite particles that reach the outer rim of the sand bed will diffuse into the boundary layer of the seeping water. The diffusivity of smectite particles is orders of magnitude lower than that of ionic species. During a given time they move a short distance into the seeping water. When the water has passed the deposition hole it has picked up a limited amount of colloids. This can be thought of as a resistance to colloid transfer to the seeping water. However, at the downward sloping part of the fracture, gravitation helps to pull the sol particles down into the water. At the lower end of the fracture, the rate of loss of smectite is therefore faster than at the upper parts.

One may speculate on the fate of the sand. At least the sand particles that are larger than the smectite particles will tend to sediment to the bottom of the fracture eventually filling a section below the deposition hole with sand. Water flowrate will decrease there and slow down the rate of transport of the smectite particles.

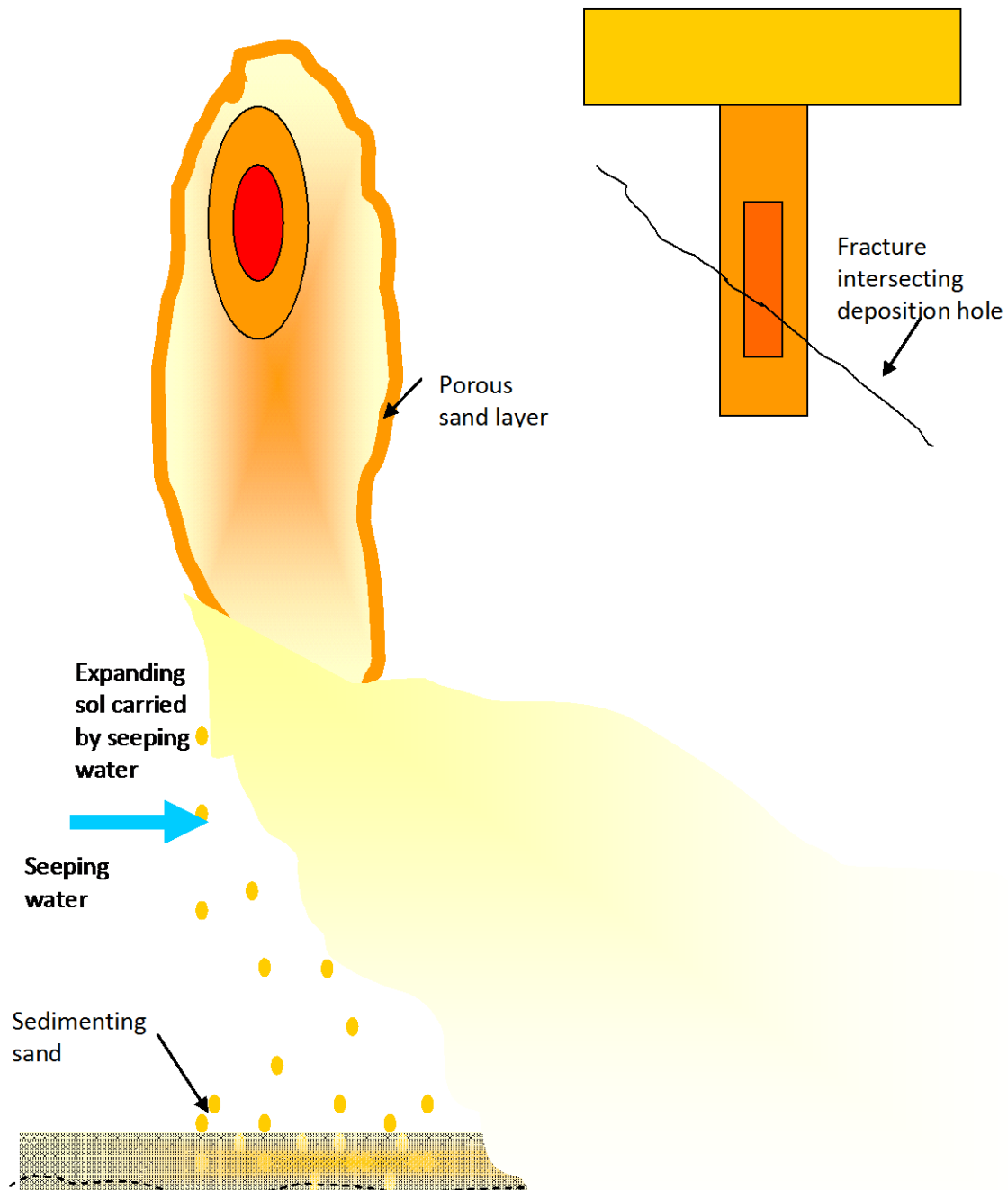


Figure 2-7 Cartoon of how a sand region could develop in the fracture around a deposition hole and that it may be breached and sediment away in the lower parts of the fracture.

2.5 Erosion experiments

A series of erosion experiments were performed in which compacted bentonite was subjected to flowing water in a thin slit by Schatz et al. (2012). The pictures below are taken from their report. The principle is shown in Figure 2-8.

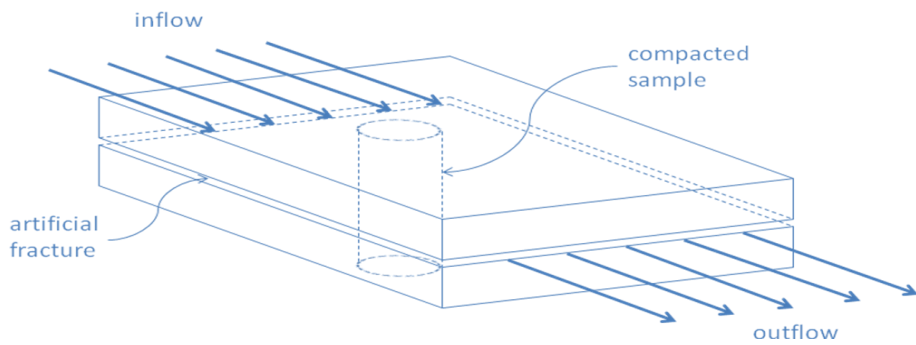


Figure 2-8 Schematic representation of the flow-through, artificial fracture test system design basis.

Experiments were performed with water compositions below and above the CCC. Homo-ionic Na and mixed 50/50 Na/Ca smectites were used. Some experiments were run from 456 to 1152 hours with different flow velocities. In some experiments the water composition was changed stepwise and these runs had durations of 2688 hours. The expansion of the clay into the slit was photographed.

Figure 2-9 shows the expansion for water with 171 mM NaCl solution passing a Na-smectite body with an original density of $\sim 1.6 \text{ g/cm}^3$. The smectite plug was 2 cm in diameter and height. The slit with the water intersected the plug at mid height. The water velocity is $2 \times 10^{-4} \text{ m/s}$. The plug was simultaneously wetted from the lower and the upper side and from the slit when the experiment started. The eroded mass in this experiment was less than 2%. In a similar experiment with 17 mM NaCl no erosion was detected. In this experiment a dye was also injected at the end of the experiment. This is shown in Figure 2-10.

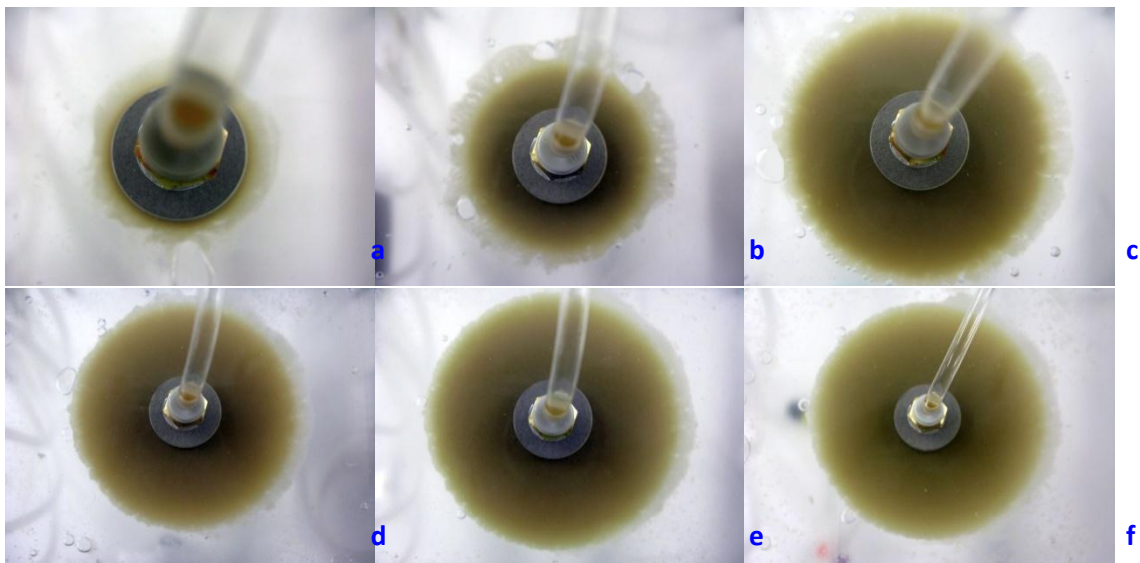
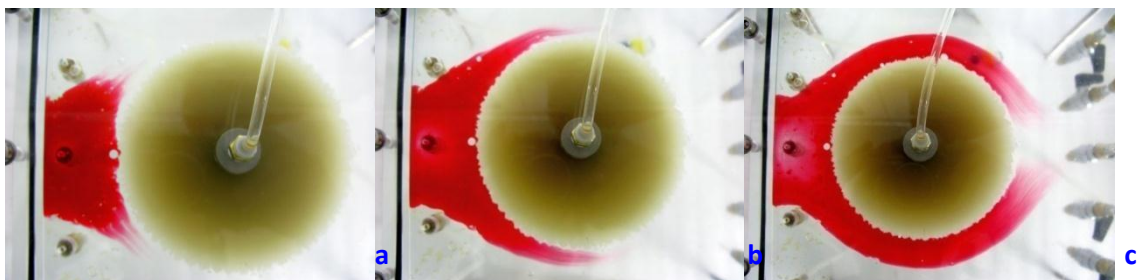


Figure 2-9 Overhead photographic images of test 1 at a) 4 h, b) 48 h, c) 168 h, d) 336 h, e) 504 h, and f) 720 h; the direction of flow in the 1 mm fracture is from left to right throughout the series. Note the porous frit (diameter = 2 cm) at the center of each image for scale.



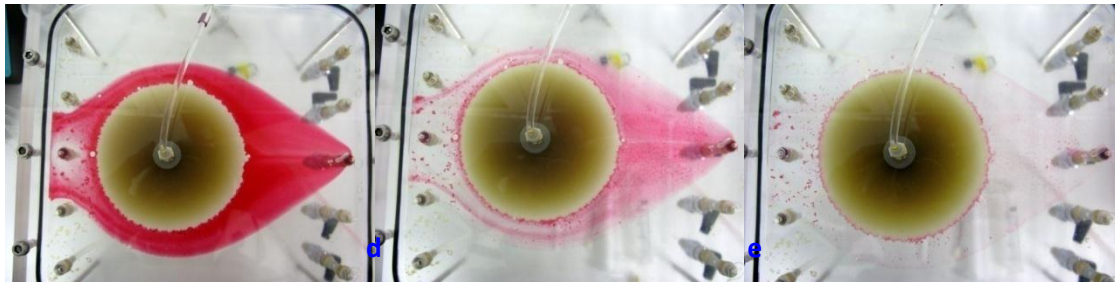


Figure 2-10 Overhead photographic images of flow visualization of test 2 at, approximately, a) 2 min, b) 4 min, c) 8 min, d) 17 min, e) 1 h, and f) 24 h after dye injection; the direction of flow in the 1 mm fracture is from left to right throughout the series.

It is clearly seen that the interface between the gel and the seeping water is very sharp. The equipment was turned from horizontal to vertical to see if the gel would be influenced by gravity but it was not. The NaCl concentration in this experiment was 10 mM. The NaCl concentration is expected to be below the CCC according to the model described earlier

In a test with de-ionised water the erosion was clearly seen. This is shown in Figure 2-11.

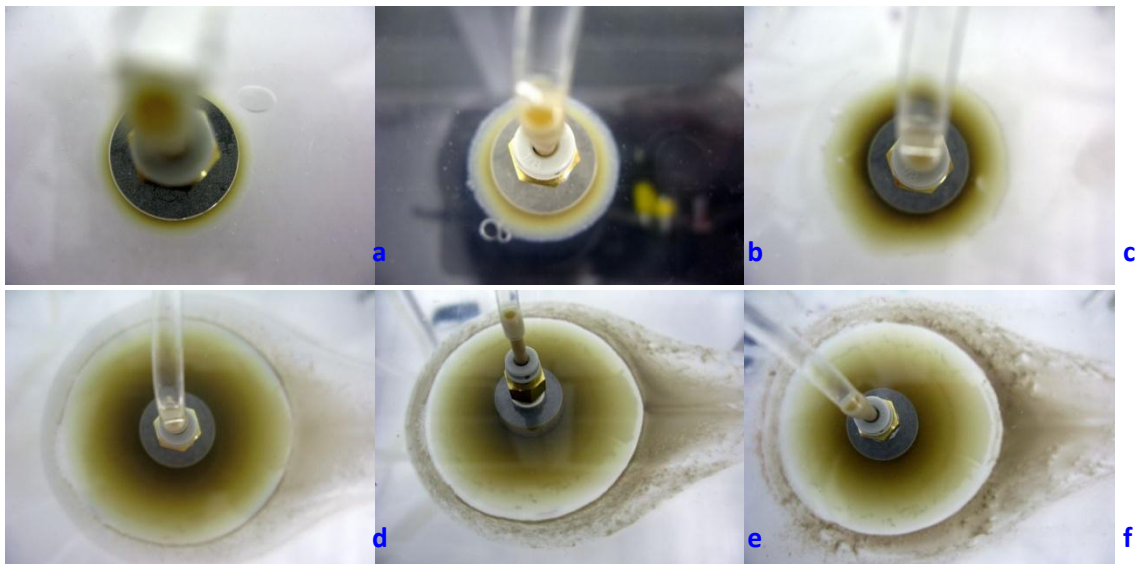


Figure 2-11 Overhead photographic images of test 3 at a) 1 h, b) 4 h, c) 24 h, d) 144 h, e) 312 h, and f) 456 h; the direction of flow in the 1 mm fracture is from left to right throughout the series. Note the porous frit (diameter = 2 cm) at the center of each image for scale.

It may be noted that the gel even in this case expands radially with near symmetry and that there is a very sharp boundary between the gel and the mobile sol. This is shown in Figure 2-12.

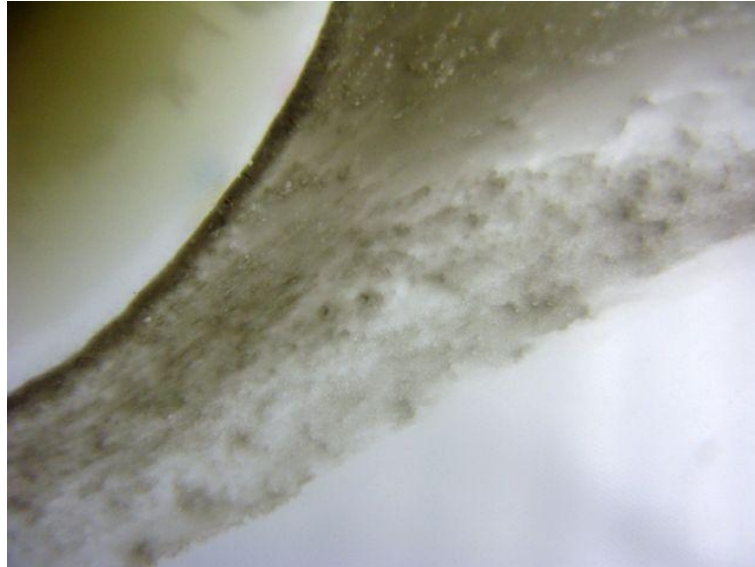


Figure 2-12 Close-up photographic image of test 3 at 456 h showing the interface between the inner zone of extruded material and the outer zone of eroding material.

Of special interest is that when the equipment was turned 90 degrees the eroded smectite sedimented rapidly. Figure 2-13 shows this.

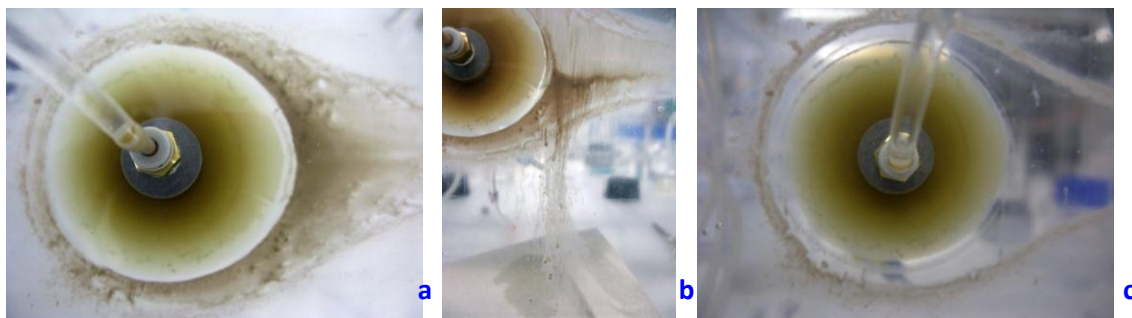


Figure 2-13 Photographic images of test 3 a) before, b) at 90° rotation from a horizontal fracture position to vertical, and c) after 1 h.

The eroding material rapidly sediments with gravity. Such sedimentation is indicative of particle sizes larger than those in the colloidal size range ($< 2 \mu\text{m}$). The extruded material, on the other hand, shows complete, static resistance to flow under gravitational load similar to the behaviour observed in tests 1 and 2. Similar behaviour was obtained with simulated groundwater with the same Na and Ca concentration as Grimsel water.

The release of smectite from the gel is seen to be affected by gravity also in other tests. Figure 2-14 shows a close-up of a test with deionized water and a 50/50 mix of Na and Ca smectite.

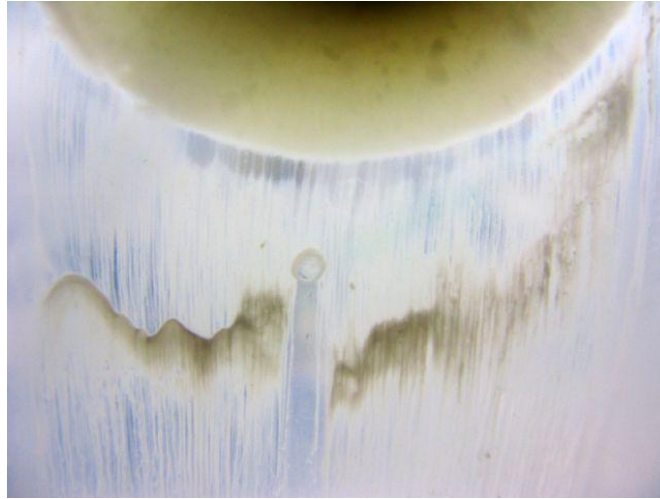


Figure 2-14 Close-up photographic image of test 9 at 90° rotation from a horizontal fracture position to vertical.

The release seems to be taking place in very narrow streams. Such behavior is not predicted by the dynamic model described earlier or other models describing bentonite erosion. In the dynamic model the smectite particles are released forming a sol and they are very little affected by gravity. The phenomena shown in Figure 2-11 and Figure 2-12 showing a grainy gel/sol and especially in Figure 2-13 and Figure 2-14 suggest that the smectite particles form larger particles with low volume fractions of smectite, which because of their larger mass sediment rapidly. The phenomenon shown in Figure 2-14 reminds of the Rayleigh-Taylor instability, (http://en.wikipedia.org/wiki/Rayleigh-Taylor_instabilityDiscussion). Such instability can cause rapid fingering to develop. Similar observations were made by Jansson (2009) who showed that smectite particles, in below CCC conditions, rapidly sedimented through a very fine net. A mass of 0.2 g of homoionic smectite sedimented through the 17 micrometer mesh size net in about 10 minutes. Figure 2-15 shows an example of these experiments. A 3 mM CaCl_2 solution did not allow the smectite to pass the filter whereas 1 and 2 mM readily let the particles pass pulled by gravity.

These observations suggest that the erosion model proposed by Moreno et al. (2009) may underestimate the rate of release of smectite to seeping water with ionic strengths below a few mM of either Na or Ca. The cluster/slurry formation can be hypothesized to be caused by edge to face attraction. Such flexible, non-rigid structures could conceivably wriggle through narrow passages. Such structures could also conceivably act as liquid slightly denser than water and be subject to the Rayleigh-Taylor phenomenon.

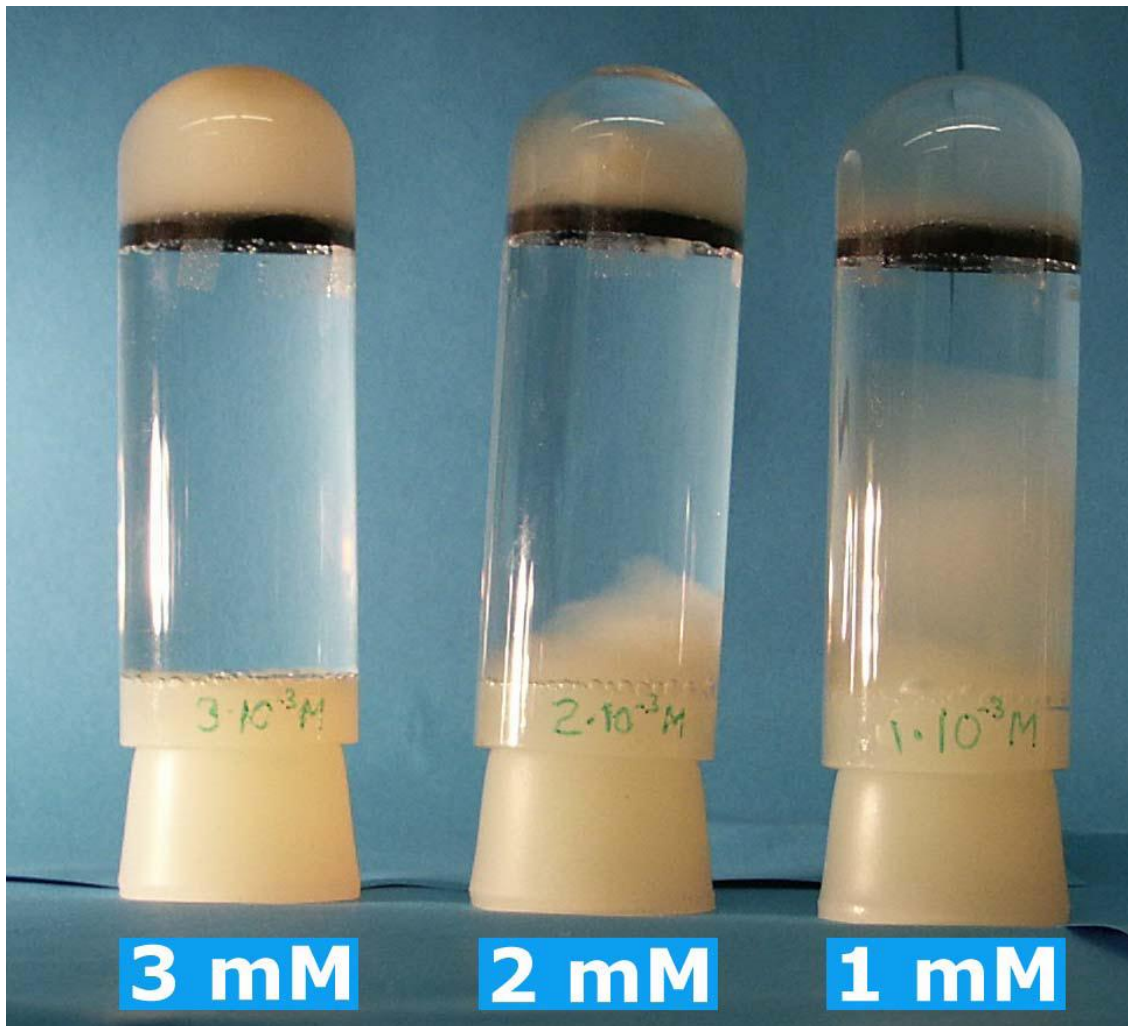


Figure 2-15 Determination of lowest calcium concentration needed to keep homoionic sodium smectite from dispersing. From Jansson (2009)

2.6 Calcium dominated smectites

Another area where the phenomena are not fully understood is the behaviour of calcium-dominated smectites. Very calcium rich smectites can behave very differently from sodium-dominated clays. The former are known to form stacks of sheets strongly held together by ion-ion correlations. Nevertheless, the stacks repel each other nearly as strongly as the individual sheets in sodium clays. The reasons are not understood. See BELBaR deliverable 4.3 of May 27 this year.

A simple hypothetical model is proposed where the outer sheets of the stack behave as if they are sodium dominated. This would lead to repulsion between the stacks similar or equal to that of the individual sheets in sodium dominated clay. The DDL repulsion force would be the same for the same distance between stacks as for sheets. The stacks would swell to the same distance between the outer sheets on the stacks as the distance between the individual sheets in sodium clays, if restrained by the same force e.g. gravity or vdW forces. The large stacks would be less prone to leave the gel by Brownian movement because of their larger mass. Sol formation would be more difficult.

This hypothetical model does not explain why the stacks are formed with the outer sheets behaving essentially as sodium charged sheets when the inner sheets in the stacks are strongly attracted by ion-ion correlations. However, it would explain why calcium dominated clay stacks have essentially the same swelling pressure at high volume fractions. It also explains why calcium clay expands more rapidly initially as the stacks have smaller surface to volume ratio and thus are less restrained in their

movement against the water that intrudes the gel to replace the volume vacated by the stack. The friction force per mass of particle is smaller. It furthermore explains why calcium gel stops expanding at a larger clay volume fraction when the stacks reach the distance when the attractive van der Waals forces balance the repulsive DDL forces. The latter is conditioned on the ionic strength being sufficiently high that it is above the CCC. Below the CCC vdW forces will not be strong enough to balance the DDL forces at any stack/sheet distance. The individual sheets of sodium smectite might be able to release particles by thermal forces- Brownian movement- and form a stable sol. This does not seem to be observed, however. The much more massive stacks are not be released as readily. In upward expanding experiments gravity has a much stronger effect on the larger stacks and pulls back the stacks more strongly. The above hypothetical model suggests that also calcium gel in de-ionized water should expand “forever”, forming a sol, when allowed to expand horizontally. The gravity then plays no role. The sol formation would be much slower, however, than for sodium clays as the “diffusivity” of the large stacks is much smaller than for individual sheets. We have found no long-term experiments described in the literature to support this, however. Hopefully some of the experimental teams in BELBaR can be stimulated to make such experiments.

2.7 Discussion

Erosion of bentonite gels by seeping water in narrow fractures are not likely to occur if the water composition at the gel/water interface is above the CCC. In waters with Na and Ca concentrations below a few mM the gel can release smectite particles to the water, which can carry them away. There is a good understanding of several of the key phenomena that influence erosion processes under flowing water conditions as has been described above. However, there are other processes that experiments have shown not to be so well understood that they can be used in models to quantitatively predict erosion rates. On the other hand there are phenomena that could slow down and even hinder the erosion that have not been well investigated.

The observed release of particles in flow experiment by Schatz et al (2012) show that the eroding gel does not form a homogeneous sol as expected by the dynamic model. A dilute inhomogeneous suspension of agglomerating particles forms which rapidly sediments when exposed to gravity. The properties of the suspension are not understood, nor the underlying mechanisms. With the present lack of understanding of the properties of the dilute gel/slurry it cannot be ruled out that the formation and sedimentation of the slurry could increase erosion.

On the other hand the impact of the presence of the detritus material is not credited in the models. If it can be shown experimentally and supported by modelling that the detritus is bound to clog the variable aperture fractures and form filters for smectite this can be expected to strongly decrease the erosion.

The behaviour and properties of calcium rich smectite is not well understood. Although it is observed that pure homo-ionic calcium smectite does not erode it is found that only a few tens of % of sodium as counter ions makes it release colloids as sodium smectites do. The theoretical understanding of Ca smectite behaviour in this respect is not complete.

2.8 References

Birgersson M., Börgesson L., Hedström M., Karnland O., Nilsson U., (2009), Bentonite erosion, Final Report, SKB Technical report TR-09-34

Dvinskikh, S. V. and Furó, I., (2009), Magnetic resonance imaging and nuclear magnetic resonance investigations of bentonite systems, SKB Technical Report TR-09-27

Dvinskikh S.V., Szutkowski K., Furó I., (2009), MRI profiles over very wide concentration

ranges: application to swelling of a bentonite clay, *J. Magn. Res.* 198, 146–150

Jansson M., (2009), Bentonite erosion-Laboratory studies. Technical Report TR-09-33,

Liu L., Neretnieks I., (2008), Homo-interaction between parallel plates at constant charge, *Colloids Surf. A: Physicochem. Eng. Aspects* 317, 636–642

Liu L., Moreno L., Neretnieks I., (2009a), A dynamic force balance model for colloidal expansion and its DLVO-based application, *Langmuir* 25, 679–687

Liu L., Moreno L., Neretnieks I., (2009b), A Novel Approach to Determine the Critical Coagulation Concentration of a Colloidal Dispersion with Plate-like Particles, *Langmuir*, 25 (2), 688-697 • DOI: 10.1021/la802658g •

Liu L., (2011), A model for the viscosity of dilute smectite gel, *Physics and Chemistry of the Earth* 36 1792–1798

Liu L., (2010), Permeability and expansibility of sodium bentonite in dilute solutions, *Colloids and Surfaces A: Physicochem. Eng. Aspects* 358, 68–78

Liu L., Neretnieks I., Moreno L., (2011), Permeability and expandibility of natural bentonite MX-80 in distilled water. *Physics and Chemistry of the Earth*, 36, p 1783-1791

Neretnieks I., Liu, L., Moreno L., (2009), Mechanisms and models for bentonite erosion. SKB Technical Report TR-09-35

Richards T., Neretnieks I., (2010), Filtering of clay colloids in bentonite detritus material. *Chem. Eng. Technol.*, 33, No 8, 1303-1310

Schatz, T., Kanerva, N., Martikainen, J., Sane, P., Olin, M., Seppälä, A and Koskinen, K., (2012). Buffer Erosion in Dilute Groundwater. Posiva Report 2012-44

3 Erosion experiments under flow conditions: CIEMAT

Ursula Alonso, Tiziana Missana

To elucidate the mechanisms, and the main chemical and physical factors, affecting the formation of colloidal particles at the compacted bentonite barrier surface in deep geological repositories for high-level radioactive waste, different experiments were developed at CIEMAT.

Experiments were designed with confined and compacted bentonite, simulating repository conditions. In a repository scenario, the water coming from the geological formation hydrates the bentonite and promotes its swelling. Due to its expansion, bentonite suffers a density loss, strongest at the gel front and, under favorable conditions; the gel can be transformed to sol. Bentonite particles release can be chemically induced (*static conditions*) or mechanically produced, when water flows along the bentonite surface (*dynamic conditions*).

Colloid erosion experiments were mainly carried out with natural raw FEBEX bentonite, a Na-Ca-Mg bentonite with 92% smectite content and a 30 % of exchangeable Na (Huertas et al, 2000). First experiments carried out under quasi-static conditions demonstrated that particle erosion can be chemically induced (Missana et al, 2003). It was observed that the extrusion of the clay from the compacted barrier resulted in a local loss of density leading to clay colloid (diameters around 300 nm) detachment, but quantification of the colloidal source term in a repository containing bentonite barriers deserved further investigation.

Studies carried out under static conditions, demonstrated the relevance of clay compaction density (1.2-1.6 g/cm³), main exchangeable cation and the water chemistry on colloid generation masses. Colloid erosion results, obtained under static conditions with different bentonite (raw FEBEX and Na and Ca homoionic bentonite) and different electrolytes, showed that an initial fairly linear erosion rate exists but the system, if conditions are not changed, tends to achieving an equilibrium. The maximum generation masses were both dependent on the clay properties (main exchangeable cation, compaction density and bentonite type), on the water conditions (chemical composition, Ca content and ionic strength) and on the extrusion path area (Alonso et al. (2007), Albarran et al. In press).

To study colloid erosion under flow conditions, from compacted and confined clay, the experimental set-up presented in Figure 1 was used (Missana et al., 2011).

Approximately 46 grams of FEBEX bentonite was compacted to a density of 1.65 g·cm⁻³ in cylindrical pellets (5 cm of diameter and 1.24 cm of thickness) and installed in the experimental cell, in which one surface that includes a sintered steel filter is exposed to the water flow and the other surface is closed. A large reservoir (in-reservoir) contained the initial aqueous solution that entered into the cell through Teflon tubing. The solution was forced through the sintered steel filter with a peristaltic pump and periodically collected after the contact with the bentonite surface, for colloids and chemical analysis (Figure 3-1). The water eluted was collected in polyethylene tubes of 20-60 mL. The collected water was analyzed by Photon Correlation spectrometry (PCS), to determine the size and concentration of eroded particles, as described in (Missana et al, 2003; 2011). The experimental set-up allows performing generation experiment under different chemical and hydrodynamic conditions.

First erosion studies, under constant flow conditions ($v = 1.2 \cdot 10^{-7}$ m/s) were carried out with compacted FEBEX bentonite at 1.65 g/cm³ and with different electrolytes (NaCl, mixed Ca and Na electrolyte and CaCl₂ at 10⁻³ M). Figure 3-2 shows the accumulated colloid masses eroded in the different electrolytes. Results suggested a continuous linear erosion rate, within experiments that lasted 200 days. These rates were dependant on initial electrolyte, higher rates measured in Ca-free

electrolytes, with maximum erosion rate in NaCl electrolyte of $2.6 \cdot 10^{-2} \text{ Kg/y} \cdot \text{m}^2$ (Missana et al, 2011; Albarran et al, In Press).

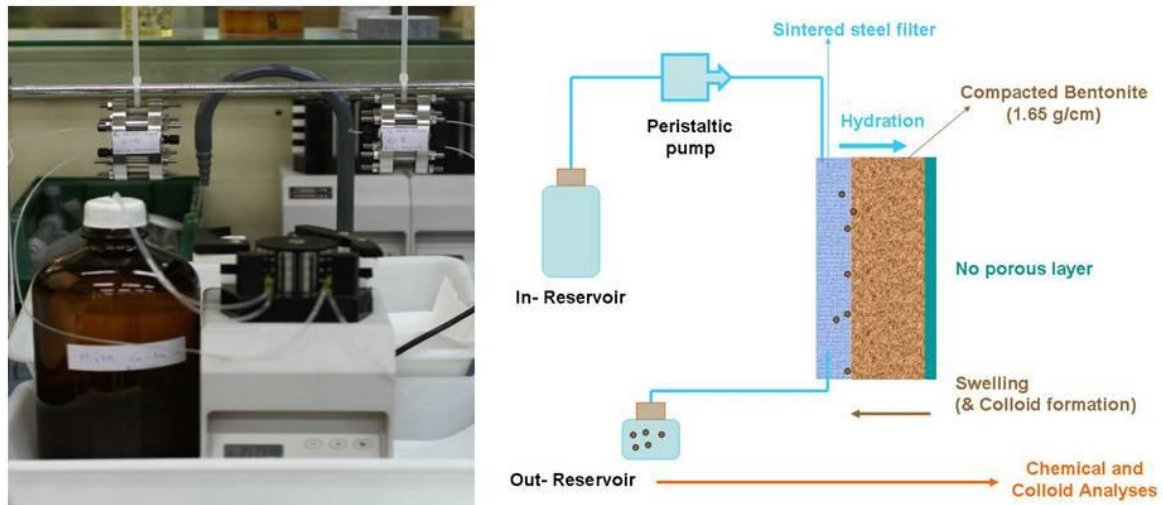


Figure 3-1 CIEMAT experimental set-up to study bentonite erosion from confined and compacted bentonite under different flow conditions.

Constant and continuous bentonite erosion would imply that the barrier integrity could be compromised at the long timescales of a repository. Therefore, to check whether the erosion remained constant at longer experimental times and to extend the study to different flow velocities was considered necessary.

Longer experiments (450 days) were also carried out with FEBEX bentonite compacted at a density of 1.65 g/cm^3 and with NaCl and a mixed Ca-Na electrolyte at 10^{-3} M . Figure 3-3 shows the accumulated eroded masses measured under lower initial flow rate ($1.2 \cdot 10^{-8} \text{ m/s}$) than in previous experiments (Figure 2). Results confirmed that initial erosion rates were fairly constant with time, but at longer time the erosion was slowed down. In the case of electrolytes with Ca content eroded mass tended to equilibrium, as can be appreciated in Figure 18, but the effects were not so evident with NaCl electrolyte, which just showed gentle variations on colloid erosion rhythm under the experiment time span. It is also noteworthy that significant changes in colloid erosion rates were not observed, when the flow conditions were increased to $1.2 \cdot 10^{-7} \text{ M}$.

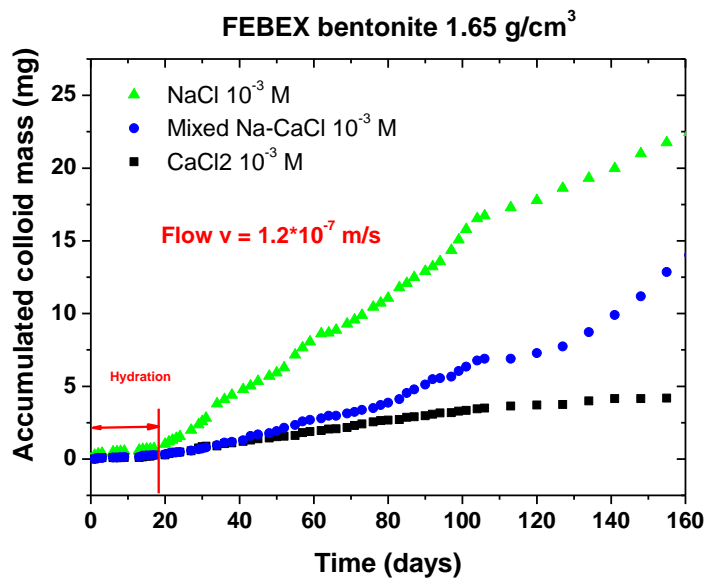


Figure 3-2 Accumulated colloid mass in $1 \cdot 10^{-3}$ M NaCl, $1 \cdot 10^{-3}$ M Mixed and $1 \cdot 10^{-3}$ M CaCl₂ at water flow rate velocity of $1.2 \cdot 10^{-7}$ m in experiments that lasted 200 days (Albarran et al. In Press).

The possibility that physico-chemical conditions change over time cannot be ruled out considering the lifetimes of a repository. Thus, it was considered necessary to carry out generation experiments in systems where the equilibrium was already reached, in which successive changes in water chemistry, or flow rates were applied. Figure 3-4 shows the accumulated masses eroded from to equal cells with FEBEX bentonite subjected to different consecutive flow changes with mixed Ca and Na electrolyte at 10^{-3} M. The cells were subjected to consecutive flow changes, applied during selected time periods, with water velocities varied from $1.5 \cdot 10^{-8}$ m/s to $3.5 \cdot 10^{-6}$ m/s. Experiments lasted more than 3 years.

Results presented in Figure 3-4 show that the erosion rates measured at longer times are much lower than those observed in the initial linear stage. Significant changes in colloid erosion rates were not observed, in any case, under successive flow changes and under the experimental conditions analyzed. The system chemistry seems to be much more relevant on colloid erosion rates than flow velocity. It was observed that the continuous calcium supply inhibited colloid erosion. Both findings limit colloid erosion effects on the bentonite barrier integrity. The important effect of ionic exchange on bentonite erosion rates is pointed out. Thus, also under dynamic flow conditions, erosion seems to achieve a maximum possible value, depending on the conditions of the experiments, as was observed in static tests (Alonso et al, 2007; Missana et al, 2011).

The maximum erosion rates measured under different experimental conditions are summarized in Table 3-1. The values are normalized to the bentonite surface area exposed to water hydration ($19.6 \cdot 10^{-4}$ m²).

Results indicated that, even under flow conditions, there is a maximum threshold of colloid generation of colloids, for given initial conditions, dependent on the characteristics of the gel layer initially formed and on the feasibility of its transport.

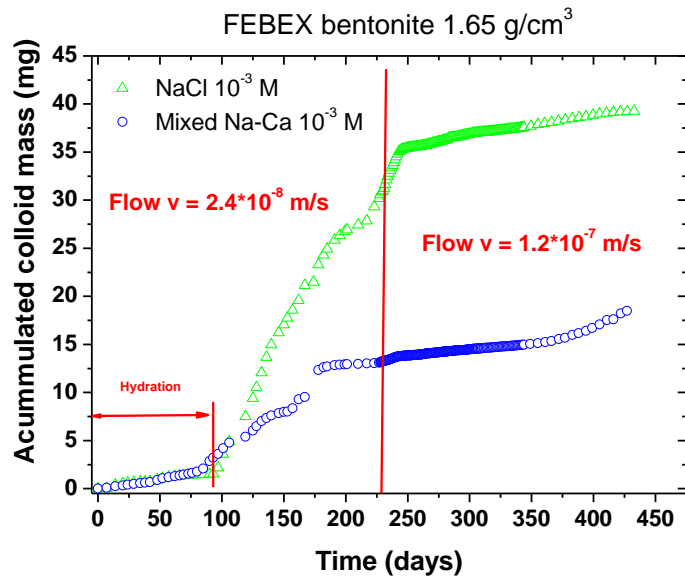


Figure 3-3 Accumulated colloid mass eroded from FEBEX bentonite in 1·10⁻³ M NaCl, 1·10⁻³ M Mixed Na and Ca electrolytes, Initial flow velocity 2.4·10⁻⁸ m/s and after 228 days flow velocity changed to 1.2·10⁻⁷ M.

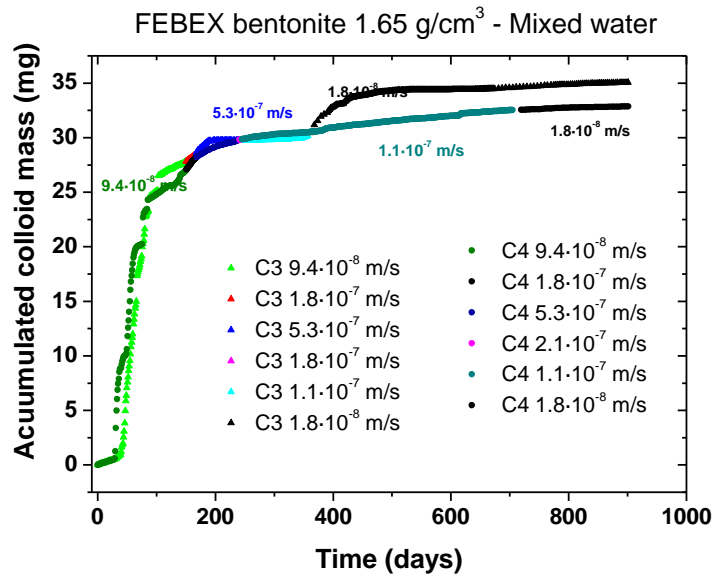


Figure 3-4 Accumulated colloid mass eroded from FEBEX bentonite in 1·10⁻³ M Mixed Na and Ca electrolyte, upon consecutive flow velocity changes.

Table 3-1 Maximum eroded rates measured under different experimental conditions (in Kg/y·m²).

EROSION RATES Kg/y·m ²					
Flow velocities	INITIAL	CONSECUTIVE FLOWS			
	1.1E-7 m/s	1.8E-7 m/s	5.3E-7 m/s	1.1E-7 m/s	1.8E-8 m/s

NaCl 10⁻³ M	3.94E-02	***	***	***	***
Mixed Na-Ca 10⁻³ M	1.22E-02	7.70E-03	5.20E-03	1E-03 - 0	1E-03 - 0
CaCl₂ 10⁻³ M	6.00E-03	****	***	***	***

References

Albarran, N., Degueldre, C., Missana, T., Alonso, U., García-Gutiérrez, M., Lopez, T. Size distribution analysis of colloid generated from compacted bentonite in low ionic strength aqueous solutions. *Applied Clay Science* (In press).

Alonso, U., Missana, T. and García-Gutiérrez, M.. Experimental approach to study the colloid generation from bentonite barrier to quantify the source term and to assess its relevance on the radionuclide migration. In: D. Dunn, C. Poissot and B. Begg (Editors), *Material and Research Society*, Boston, EEUU, pp. 605-610 (2007).

Huertas F. et al. (more than 20 authors) (2000). FEBEX Project final Report. EUR 19147.

Missana, T., Alonso, U., Turrero, M.J. Generation and stability of bentonite colloids at the bentonite /granite interface of a deep geological radioactive waste repository: *Journal of Contaminant Hydrology*, v. 61, p. 17-31 (2003).

Missana, T., Alonso, U., Albarran, N., García-Gutiérrez, M. and Cormenzana, J.L. Analysis of colloids erosion from the bentonite barrier of a high level radioactive waste repository and implications in safety assessment. *Physics and Chemistry of the Earth*, 36(17-18): 1607-1615 (2011).

4 Erosion processes under flowing water conditions (B+Tech)

Tim Schatz

4.1 Background

This report summarizes research conducted at B+Tech during the first 15 months of the BELBar Project. The work described below is related to BELBaR deliverable D2.2 “Progress report on erosion processes under flowing water conditions” and covers factors other than water chemistry and clay chemistry (which are described in BELBaR deliverable D2.1 “Report on the effects of water chemistry and clay chemistry on erosion processes”) affecting erosion.

The work at B+Tech is conducted mainly using small-scale, flow-through, artificial fracture systems in which swelling clay material can extrude/erode into a well-defined, intersecting fracture (see Figure 4-1). These experiments are performed in order to simulate the potential extrusion/erosion behavior of bentonite buffer material at a transmissive fracture interface. Using such systems the effect of solution chemistry (salt concentration and composition), material composition (sodium montmorillonite and admixtures with calcium montmorillonite, natural bentonites), flow velocity, fracture geometry (aperture, down-slope) and the role of accessory minerals on erosion processes can be analyzed.

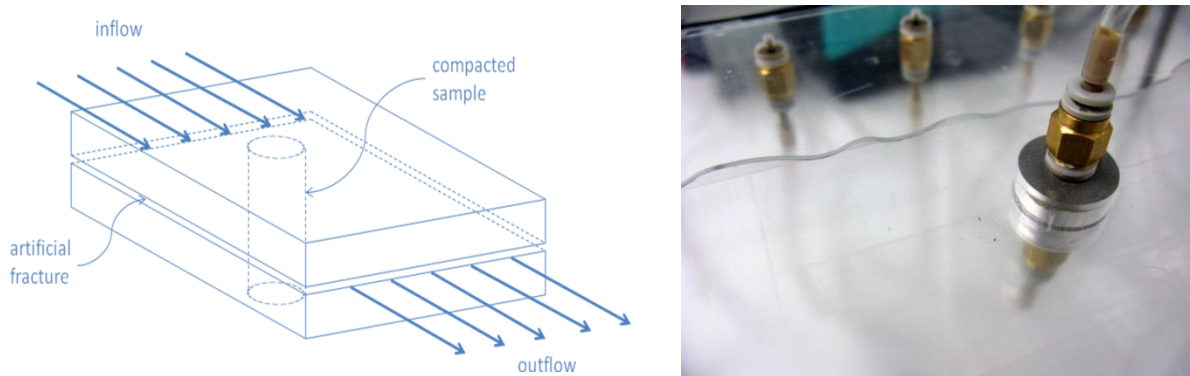


Figure 4-1 Schematic representation of the flow-through, artificial fracture test system design basis (left) and photographic image of a flow front approaching a compacted sample through a 1 mm aperture fracture (right).

4.2 Response to flow velocity and flow interruption

As discussed in BELBaR deliverable D2.1, our work shows that in contact with highly dilute solutions, i.e., $IS \leq 1.1$ mM, both sodium montmorillonite and 50/50 calcium/sodium montmorillonite samples are the most highly erodible and erode at average rates that are equivalently correlated with flow velocity (see Figure 4-2).

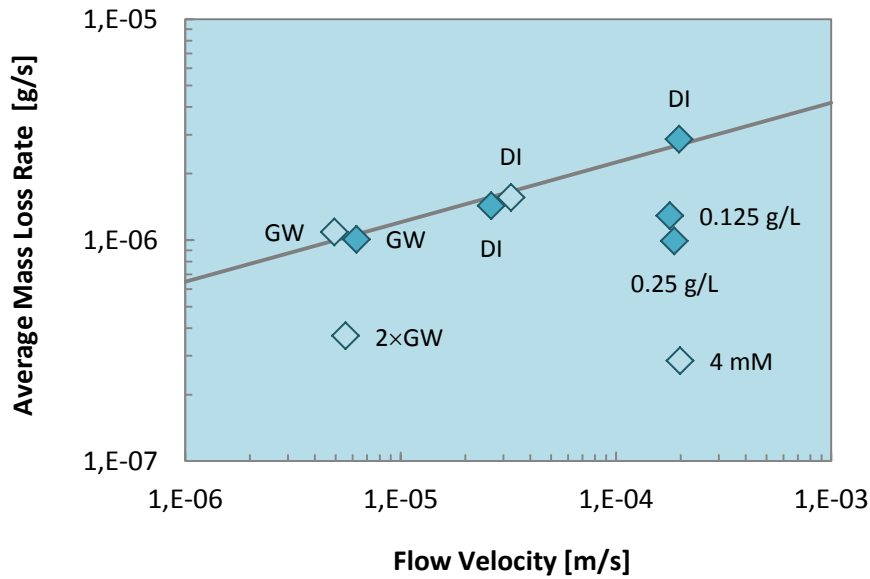


Figure 4-2 Average mass loss rates from artificial fracture experiments expressed in terms of flow velocity. Filled symbols correspond to sodium montmorillonite samples and open symbols correspond to 50/50 calcium/sodium montmorillonite samples. Data points are labelled with contact solution compositions. Limiting line (gray) though the data points for the most highly eroding systems represents power-law fit to the data.

Given the similar limiting behavior for the most highly eroding systems, this data can be used to examine more specifically the influence of flow velocity on erosion. Figure 4-3 compares the erosion results of the three, most highly-eroding, artificial fracture tests for sodium montmorillonite samples.

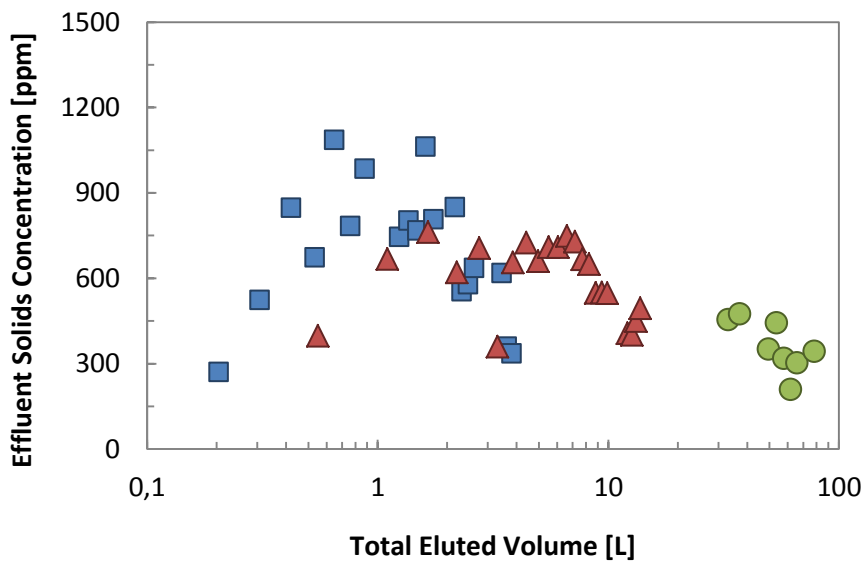


Figure 4-3 Effluent solids concentrations as a function of total eluted volume for selected artificial fracture tests performed at different flow velocities. The blue-filled squares correspond to a test performed with sodium montmorillonite against a Grimsel groundwater simulant flowing at $6 \cdot 10^{-6}$ m/s, the red-filled triangles correspond to a test performed with sodium montmorillonite against deionized water flowing at $3 \cdot 10^{-5}$ m/s and the green-filled circles correspond to a test performed with sodium montmorillonite against deionized water flowing at $2 \cdot 10^{-4}$ m/s.

As indicated in Figure 4-3, increased flow velocities lead to decreased peak effluent solids concentrations. This correlation of effluent solids concentration to flow velocity implies that the erosion of sodium montmorillonite is related to the mean residence time of water within the fracture

which suggests a rate-limited erosion mechanism at least within the range of tested flow velocities. Moreover, the observed correlation indicates that hydrodynamic shear forces are not significant.

The residence time effect was further examined by observing the erosion response to flow interruptions. Figure 4-4 shows the results from a flow interruption test with sodium montmorillonite against deionized water.

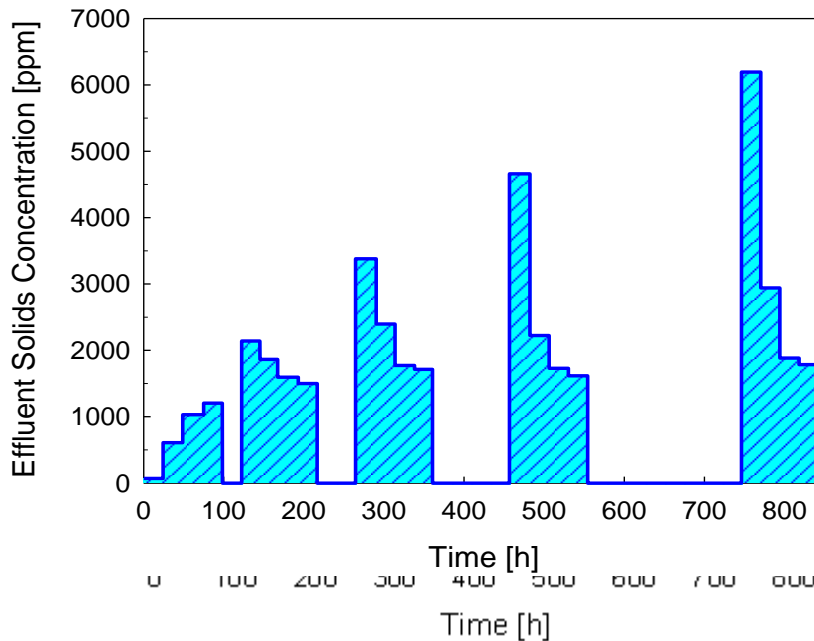


Figure 4-4 Effluent solids concentration for sodium montmorillonite against deionized water after flow interruptions of varied duration.

Clearly increased effluent solids concentrations are observed for longer flow interruptions upon resumption of flow and are related linearly. These observations provide further evidence that the erosion mechanism is rate-limited and also that the process exhibits first-order kinetics.

Based on the previous data and analysis, it can be argued that the loss of montmorillonite material in the artificial fracture experiments is governed by diffusion. Assuming that the mass transfer of montmorillonite from the periphery of the extruded material zone to the flowing solution (i.e., at the solid/liquid phase boundary) is limited to particle diffusion, the corresponding mass loss can be expressed in terms of the carrying capacity of the flowing water, i.e., the equivalent flowrate, and the density of the montmorillonite material at the interface [Moreno et al. 2010].

Using mass loss rate data from artificial fracture experiments in conjunction with the equivalent flowrate concept, particle diffusion coefficients can be extracted and compared to reference values. Preliminary calculations performed on the above basis yield diffusion coefficients on the order of 10^{-13} m²/s which is relatively consistent with theoretical and experimental values [Cadene et al. 2005, Moreno et al. 2010] and, as such, the equivalent flowrate approach may represent an experimentally verifiable route to estimating buffer mass loss due to erosion.

Artificial fracture experiments conducted at 0.1 mm aperture are also consistent with this approach in that nearly order of magnitude reduction in average erosion rates, with respect to results from 1 mm artificial fractures, are observed

4.3 Fate of accessory minerals

Following erosive loss of colloidal montmorillonite through contact with dilute groundwater at a transmissive fracture interface, accessory phases within bentonite, such as quartz, feldspar, etc., might remain behind and form a filter bed or cake. As more and more montmorillonite is lost, the thickness of the accessory mineral bed increases and the continued transport of montmorillonite slows and possibly stops if the porosity of the filter bed is sufficiently compressed. Alternatively or concurrently, as the accessory mineral filter bed retains montmorillonite colloids, a filter cake composed of montmorillonite itself may be formed. Ultimately, depending on their extent, properties, and durability, such processes may provide the bentonite buffer system with an inherent, self-filtration mechanism which serves to limit the effects of colloidal erosion.

A conceptual view of bentonite buffer extrusion and erosion in an intersecting fracture with formation of an accessory mineral filter bed and montmorillonite filter cake is presented in Figure 4-5.

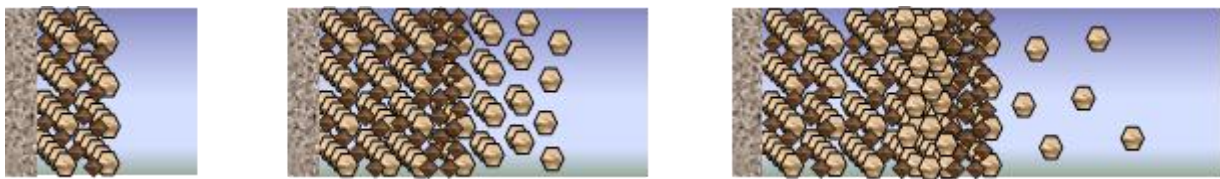


Figure 4-5 Conceptual view of a) extrusion of bentonite buffer material into intersecting fracture, b) subsequent montmorillonite erosion and accessory mineral filter bed formation, and c) montmorillonite filter cake formation. Montmorillonite colloids are represented as tan hexagons, accessory mineral particles as brown diamonds, and compacted bentonite buffer by the solid block on the left.

Due to the swelling pressure of the bentonite buffer, the situation described in Figure 4-5 may be analogous to that of the case of pressure filtration where a filter cake is formed by pressing a suspension through a filter medium and, by a mechanism known as expression, the filter cake is compressed by direct contact with a solid surface resulting in a reduction of its porosity.

In order to examine whether the erosion of bentonite material through contact with dilute groundwater at a transmissive fracture interface could intrinsically result in 1) the formation of an accessory mineral filter bed and cake and/or 2) filter caking of montmorillonite itself, a series of laboratory tests were performed in the flow-through, horizontal, 1 mm aperture, artificial fracture system. Bentonite buffer material was simulated by using mixtures (75/25 weight percent ratio) of purified sodium montmorillonite and various additives serving as accessory mineral proxies (kaolin, quartz sand, chromatographic silica). The resulting mixtures were compacted into dense sample tablets with effective montmorillonite dry densities of $\sim 1.6 \text{ g/cm}^3$. The fracture erosion tests were performed using a Grimsel groundwater simulant (relative to Na^+ and Ca^{2+} concentration only) contact solution at an average flow rate of 0.09 ml/min through the system.

The particle size distributions of the additive materials used in this study are presented in Figure 4-6. Overall the “accessory mineral” additives cover the coarse material fraction isolated from MX-80 bentonite.

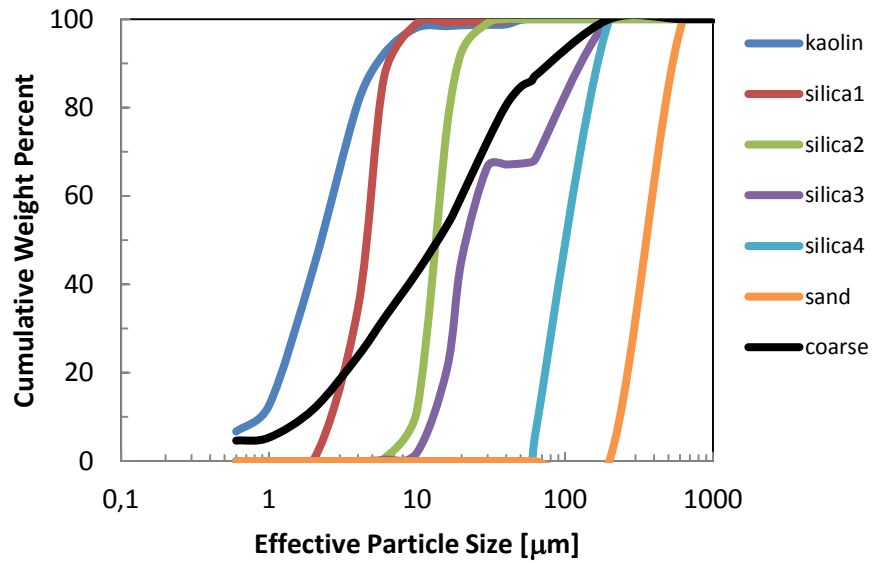


Figure 4-6 Effective particle size distribution from sedigraph analysis of the "accessory mineral" additives and isolated coarse fraction from MX-80 bentonite. See legend for details.

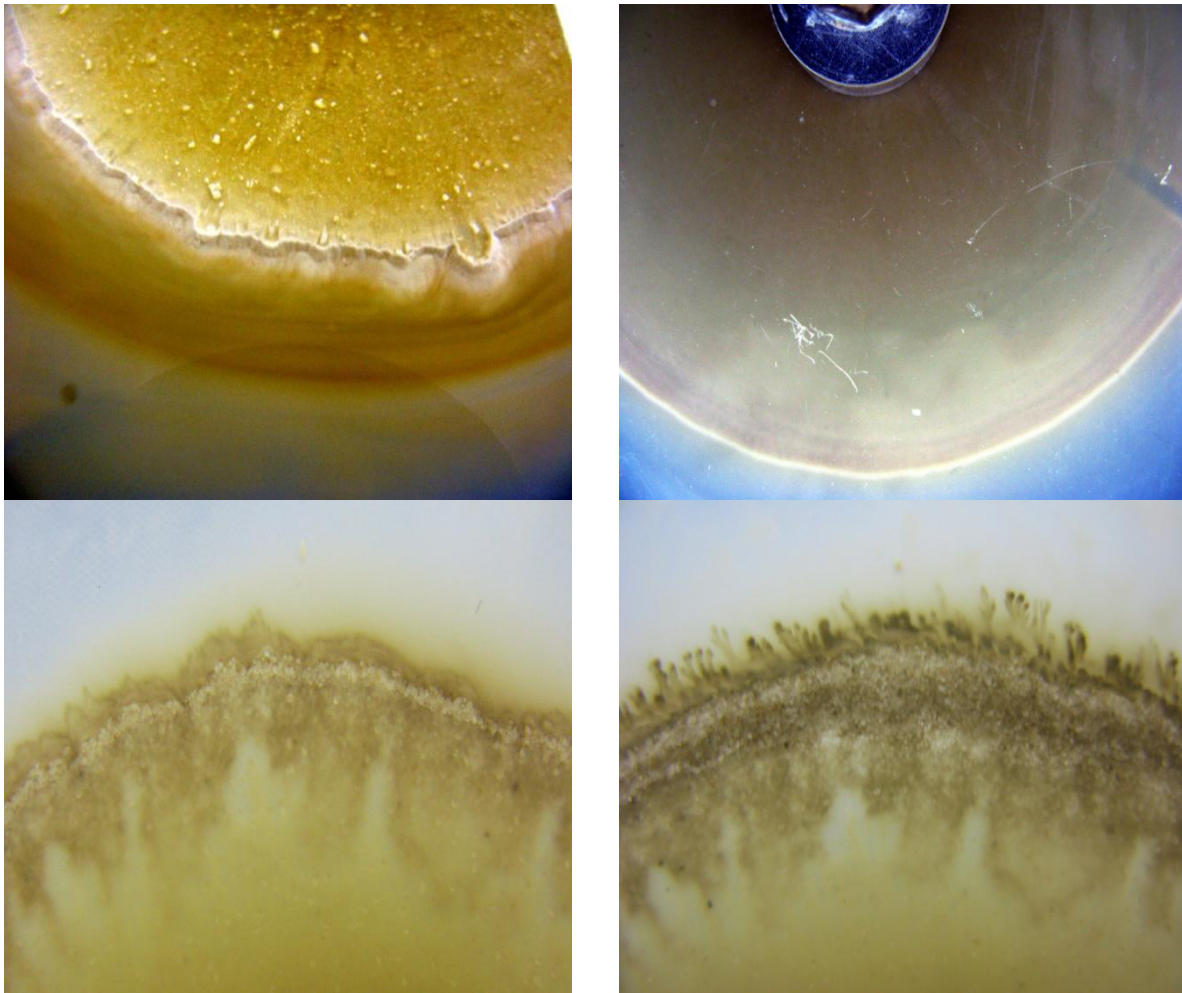


Figure 4-7 Photographic images of extrusion/erosion interface for the a) sodium montmorillonite + kaolin system , b) sodium montmorillonite + chromatographic silica 2 system, c) sodium montmorillonite + quartz sand system after 288 h of flow and d)) sodium montmorillonite + quartz sand system after 696 h of flow.

The tests were designed to lead to the development of erosive conditions (i.e., sodium montmorillonite against a dilute solution) and, in every case, the formation of an accessory mineral bed layer near the extrusion/erosion interface was observed, moreover, these layers grew progressively in thickness over the course of the tests (see Figure 4-7).

These results provide evidence that, following erosive loss of colloidal montmorillonite through contact with dilute groundwater at a transmissive fracture interface, accessory phases (within bentonite) remain behind and form bed layers. No apparent attenuation of the erosion of montmorillonite was observed in the tests with added accessory materials relative to montmorillonite alone in a 1 mm aperture fracture. Similar tests will be performed in a 0.1 mm aperture fracture for comparison.

4.4 Effect of fracture geometry

Artificial fracture tests conducted in fractures positioned at 45° slope angles for sodium montmorillonite or 50/50 calcium/sodium montmorillonite against deionized water or Grimsel groundwater simulant produce nearly identical average mass loss rates ($\pm 2\%$) that are faster the corresponding horizontal cases by almost exactly a factor of 2. Visual observations of the sloped tests indicate a seemingly, purely sedimentary mass loss mechanism (see Figure 4-8).

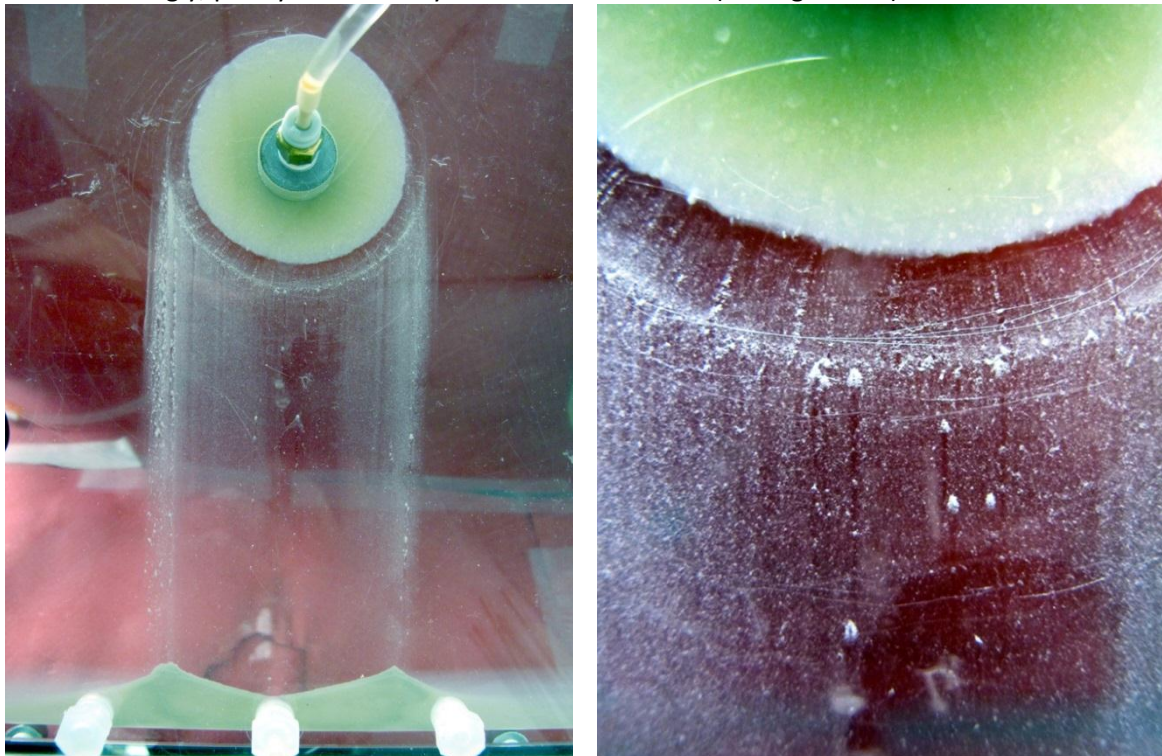


Figure 4-8 50/50 calcium/sodium montmorillonite in contact with a Grimsel groundwater simulant (relative to Na⁺ and Ca²⁺ concentration only, i.e., 0.68 and 0.14 mM, respectively) at an average flow rate of 0.09 ml/min through the 1 mm aperture artificial fracture system positioned at a 45° angle. Photos taken approximately 672 hours after start of test.

4.5 References

Cadene, A., Durand-Vidal, S., Turq, P. & Brendle, J. 2005. Study of individual Na-montmorillonite particles size, morphology, and apparent charge. *Journal of Colloid and Interface Science*. 285. 719-730.

Moreno, L., Neretnieks, I. & Liu, L. 2010. Modelling of Erosion of Bentonite Gel by Gel/Sol Flow. SKB Technical Report. TR-10-64. Svensk Kärnbränslehantering AB.

5 Bentonite erosion into the granite fracture during the saturation phase ÚJV Řež

Radek Červinka

5.1 Introduction

The main aim of our investigations was to size up the amount of bentonite particles eroded from the swelling bentonite by the flowing water in the fracture during the bentonite saturation. During the saturation phase the bentonite is not in the chemical and mechanical equilibrium with surrounding environment and the significant proportion of mechanical and chemical erosion of the bentonite can be expected (see Figure 5-1). The study was also focused on the characterization of released clay particles such as particles size distribution, size itself and stability.

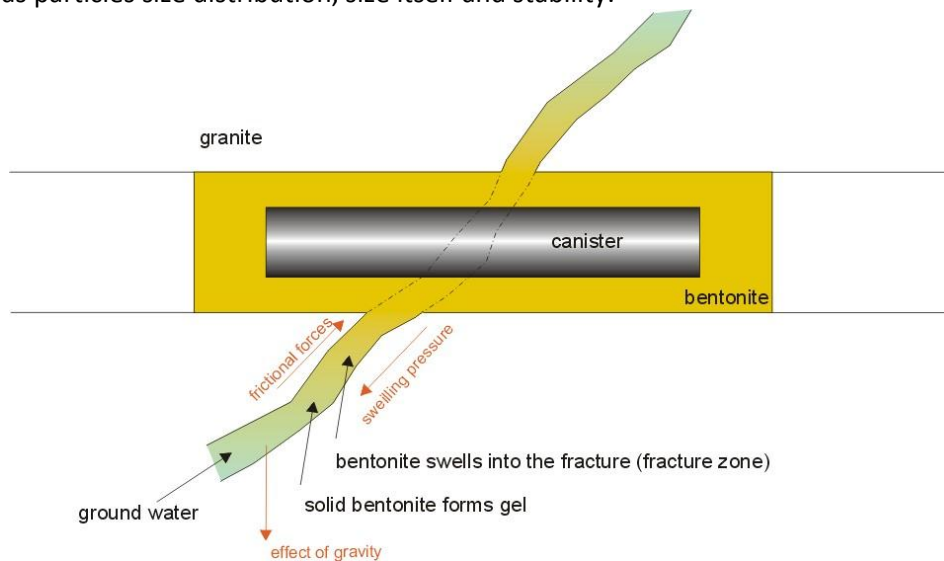


Figure 5-1 Conceptual scheme of bentonite erosion process in horizontal deposition hole.

5.2 Rokle bentonite

Besides worldwide used bentonites (MX-80, Volclay or Febex) with well known chemistry and behaviour, local Ca-Mg bentonites from Rokle deposit (CZ) with more complex mineralogy and chemistry are considered as candidate materials for both DGR buffer and backfill in czech concept. The natural Ca-Mg bentonite is processed on the production line (grinding, homogenization) and the final commercial product is denoted as Bentonite 75 (B75) and Sabenyl 65 (S65). During the process the bentonite is partly Na-activated in the case of B75 and fully activated in case of S65. Interlayer cation occupation is changed from Ca-Mg to Na-Mg (see Figure 5-2).

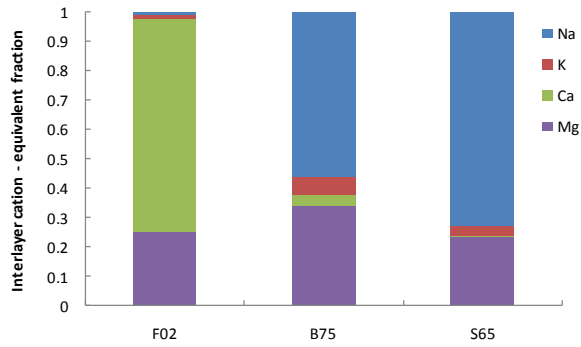


Figure 5-2 Interlayer cation occupation for three bentonites from Rokle deposit. F02 – natural bentonite, B75 – commercial product (partly Na-activated), S65 – commercial product (fully Na-activated).

5.3 Experimental set-up

An experimental device for experimental investigations was developed (Figure 5-3). The granite cylinder with longitudinal artificial fracture (orange) is surrounded by compacted bentonite (yellow). We used the compacted dry density about 1600 kg/m^3 for all experiments. Complete sample is tightly pressed in the polycarbonate ring with the pistons (grey), serving for the inlet and outlet of water (blue arrows). The water flows directly to the fracture plane and the bentonite is in contact with water only at open edges of fracture. The flow rate is maintained by peristaltic pump and outlet water is collected in reservoir with periodical sampling. The experiment was running until full saturation of bentonite was reached. In contrast with this conceptual model, the experiments consider some simplifications, because of experimental and evaluation limitations, particularly: the granite fracture had smooth inner surface without mineral infill and the water flow direction was from bottom to top. This direction allowed to fully saturate the whole volume of bentonite inside the apparatus.

The pH, conductivity, flow rate and colloids concentration was measured in effluents collected periodically. Two ways of colloid concentration measurement were used; indirectly using Al as a tracer for clay particles and directly using dynamic light scattering. Total amount of eroded bentonite was estimated gravimetrically. In all experiments Rokle bentonite (B75) and pure water was used.

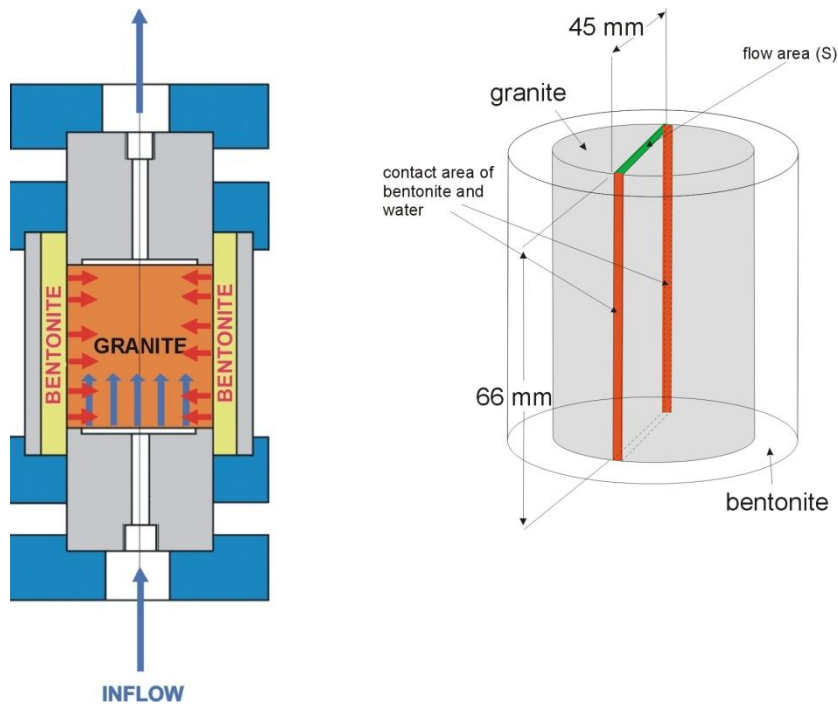


Figure 5-3 Cross section of experimental set-up (cut in the fracture plane, left). The dimensions and description of middle part with bentonite ring and granite cylinder with longitudinal artificial fracture (right).

5.4 Results

The set of erosion experiments differed particularly in aperture size of granitic fracture ($0.15 - 2 \text{ mm}$) and in flow velocity of water in granitic fracture ($1.12 \times 10^{-5} - 2.48 \times 10^{-4} \text{ m/s}$). These values are above the expected real values of flow velocity in permeable zones in czech granitic host rocks (about $1 \times 10^{-6} \text{ m/s}$ at 600 m depth). The erosion progress is illustrated in Figure 5-4. The oscillations of Al concentrations in the beginning are replaced by stable generation of clay particles after 20 days of experiments. Probably large agglomerates are carried away first and after the saturation of the contact area the generation of smaller clay particles is influenced by flowrate and in this case by low salinity of water.

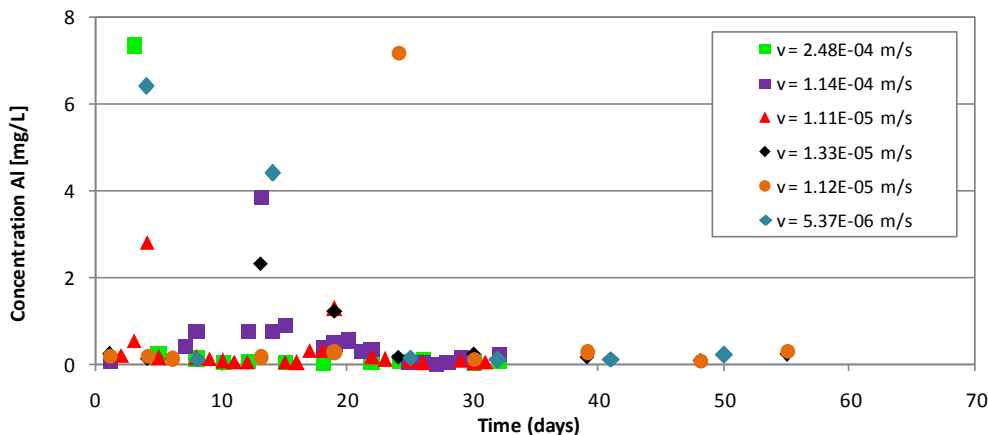


Figure 5-4 Concentration of Al (as tracer for bentonite particles) in effluent during the erosion experiments differing in water velocities.

Generally, results achieved so far do not show a clear trend between fracture aperture or flow velocity and the amount of eroded bentonite in a given experimental range. But, as expected, mostly results indicate, that with increasing fracture aperture and flow velocity increases also the eroded mass. Interesting is, that a linear trend occur between the water mass flow and the amount of

eroded bentonite. This could indicate a constant erosion rate, which is not dependent on the flow velocity within the range of measured values. The erosion rate can be recalculated to contact area of bentonite and flowing water (i.e. area of fracture). The experiments carried out show this erosion rate between 0.4 to 30.2 kg/m²/year considering the values of water velocity and fracture aperture mentioned above (in saturation phase).

The fracture aperture and entrance of swelling bentonite inside the fracture was studied by optical stereomicroscope. Also mineral phase separation occurred during the transport of eroded bentonite, mainly in settings of aperture size about 0.1-0.2 mm. The size of grains (biotite and quartz) captured in fracture plain was about 0.07 mm (Figure 5-5).

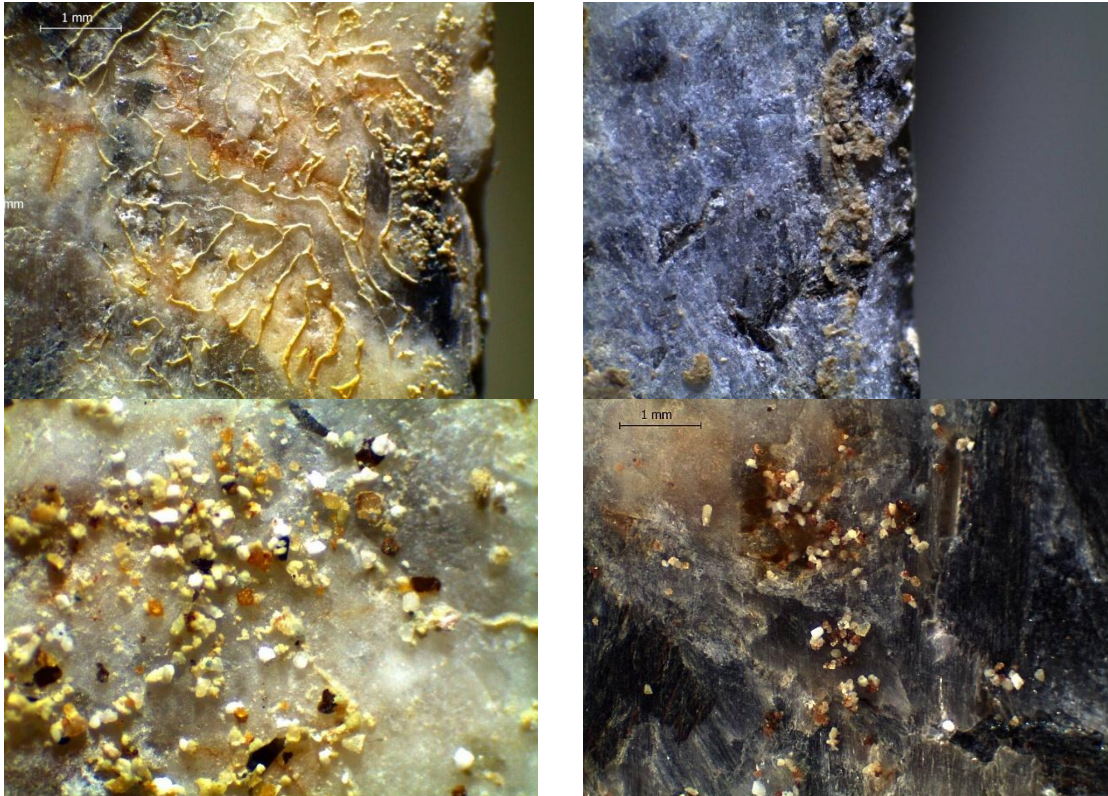


Figure 5-5 Pictures from stereomicroscopy. Penetration of swelling bentonite into the fracture (top). Mineral separation in fracture plain during the transport (bottom).